Catena 122 (2014) 180–195

Contents lists available at ScienceDirect

Catena

journal homepage: www.elsevier.com/locate/catena

Short-term geomorphic analysis in a disturbed fluvial environment by fusion of LiDAR, colour bathymetry and dGPS surveys

J. Moretto [a,*], E. Rigon [a], L. Mao [b], F. Delai [a], L. Picco [a], M.A. Lenzi [a]

[a] Department of Land, Environment, Agriculture and Forestry, University of Padova, Padova, Italy
[b] Department of Ecosystems and Environment, Pontificia Universidad Catolica de Chile, Santiago, Chile

ARTICLE INFO

Article history:
Received 11 November 2013
Received in revised form 27 June 2014
Accepted 30 June 2014
Available online xxxx

Keywords:
Fluvial processes
Gravel-bed river
LiDAR data
Colour bathymetry
Floods
DoD

ABSTRACT

Objective: Estimating river's underwater bed elevations is a necessary but challenging task. The objective of this study is to develop a revised approach to generate accurate and detailed Digital Terrain Models (DTMs) of a river reach by merging LiDAR data for the dry area, with water depth indirectly derived from aerial imagery for wet areas.
Methods: This approach was applied along three sub-reaches of the Brenta River (Italy) before and after two major flood events. A regression model relating water depth and intensity of the three colour bands derived from aerial photos, was implemented. More than 2400 in-channel depth calibration points were taken using a differential Global Positioning System (dGPS) along a wide range of underwater bed forms.
Results: The resulting DTMs closely matched the field-surveyed bed surface, and allowed to assess that a 10-year recurrence interval flood generated a predominance of erosion processes. Erosion dominated in the upper part of the study segment (−104,082 m^3), whereas a near-equilibrium is featured on the lower reach (−45,232 m^3). The DTMs allowed the detection of processes such as riffle–pool downstream migration, and the progressive scour of a pool located near a rip-rap.
Conclusion: The presented approach provides an adequate topographical description of the river bed to explore channel adjustments due to flood events.
Practice: Combining colour bathymetry and dGPS surveys proved to represent a useful tool for many fluvial engineering, ecology, and management purposes.
Implications: The proposed approach represents a valuable tool for river topography description, river management, ecology and restoration purposes, when bathymetric data are not available.

1. Introduction

The study of river morphology and dynamics is essential for understanding the factors determining sediment erosion, transport and deposition processes. Natural (e.g. climatic and hydrological variations) and anthropic factors (e.g. water captures, grade-control works, gravel mining, deforestation) can act at both the reach- and basin-scales changing the magnitude and timing of these processes (Buffington, 2012). Geomorphic variations at the reach scale are a direct consequence of sediment erosion and deposition processes, which are in turn influenced by the size and volume of sediment supply, transport capacity of the flow, and local topographic constraints. The actual ability to quantify the interaction of these processes is limited by the difficulty of collecting high spatial resolution data in river environments. Traditional approaches, based on the application of hydraulic formulas at cross-sections, fail when aimed at describing non-uniform natural conditions. Three-dimensional and high-resolution representations of river bed morphology are used in many applications such as hydraulic and cellular modelling (e.g. Rumsby et al., 2008), evaluation of climate change impacts on river systems (e.g. Rumsby and Macklin, 1994), flood hazard management (Fewtrell et al., 2011; Macklin and Rumsby, 2007; Sampson et al., 2012), assessment of erosion and deposition areas along the river corridor (Lane et al., 2007; Picco et al., 2013; Stover and Montgomery, 2001). Calculating sediment budgets, estimating transport rates, and understanding changes in sediment storage are also fundamental aspects to quantify geomorphological changes due to flood events and changes in flow regime (Ashmore and Church, 1998; Wheaton et al., 2013).

The traditional techniques of terrain survey (e.g. total station devices, differential Global Positioning System - dGPS; Brasington et al., 2000) in the evaluation of morphological changes across large areas have so far demonstrated to be expensive, time-consuming and difficult to apply in zones with limited accessibility. Some innovative methods are good alternatives for producing high-resolution Digital Terrain Models (DTMs) of fluvial systems. Recent studies on morphological channel changes have used passive remote sensing techniques such as

* Corresponding author at: Agripolis Campus, Viale dell'Università, 16. 35020 - Legnaro Padova, Italy. Fax: +39 0 498272750.
E-mail address: johnny.moretto@studenti.unipd.it (J. Moretto).

http://dx.doi.org/10.1016/j.catena.2014.06.023
0341-8162/

digital image processing (e.g. Forward Image Model, Legleiter and Roberts, 2009), digital photogrammetry (Brasington et al., 2003; Dixon et al., 1998; Heritage et al., 1998; Lane et al., 2010), active sensors including Laser Imaging Detection and Ranging (LiDAR) (e.g. Brasington et al., 2012; Hicks, 2012; Hicks et al., 2002, 2006; Kinzel et al., 2007), and acoustic methods (e.g. Muste et al., 2012; Rennie, 2012).

The main difficulty related to the production of precise DTMs with no-bathymetric sensors concerns the absorption of natural (solar) or artificial (LiDAR) electromagnetic radiation in the wetted portion of the river channels. The capacity of the electromagnetic signal to pass through water, be reflected from the bed and reach a sensor depends on water surface texture (pleating, reflexes, etc.), water column (depth and turbidity), and nature of channel bed (substrate type and presence of algae; Marcus, 2012; Marcus and Fonstad, 2008). Even if different electro-magnetic (EM) wavelengths are absorbed by water at different degrees (Smith and Vericat, 2013; Smith et al., 2012), LiDAR signal proved to be adequately reliable to assess channel topography "where flow is sufficiently shallow that water depth does not distort the laser" (Charlton et al., 2003), as lately confirmed also by Cavalli and Tarolli (2011).

Only a few tools have proved able to provide an accurate and high-resolution measure of submerged bed surface. Moreover, the precision of the surveyed data decreases as water depth increases. Bathymetric LiDAR sensors have recently been developed and should enable the survey of underwater bed surfaces. Nevertheless, they feature high costs, relatively low resolutions, and data quality comparable to photogrammetric techniques (Hilldale and Raff, 2008). Progress in LiDAR acquisition of topographic information from submerged areas has been achieved with a new technology called Experimental Advanced Airborne Research LiDAR system (EAARL), which records the full waveform of returning laser pulse. Even if this system is affected by environmental conditions (e.g. turbulence in the pool, bubbles in the water column, turbidity, and low-bottom albedo) and by post-processing algorithms, its accuracy appears comparable to what is obtained using airborne terrestrial near-infrared LiDARs (Kinzel et al., 2013; McKean et al., 2009).

Surveys of wet areas can thus be approached using two photogrammetric techniques (manual or automatic) which are able to produce a cloud of elevation points (Fryer, 1983; Rinner, 1969), or with a technique based on the calibration of a depth–reflectance relationship of images, which can be in greyscale (e.g. Winterbottom and Gilvear, 1997), coloured (e.g. Carbonneau et al., 2006; Moretto et al., 2013a; Williams et al., 2011, 2013, 2014) or multispectral (Legleiter, 2011; Marcus et al., 2003). Both solutions need a field survey, contemporary to the flight, to provide calibration depth points.

The depth–reflectance relationship can be defined using an empirical equation, using one or more bands (e.g. Legleiter et al., 2009), or according to the Beer–Lambert law. For the latter case, the amount of light absorbed by a transparent material is considered to be proportional to the distance of the light travelling through that material (Carbonneau et al., 2006):

$$I_{out} = I_{in} e^{-cx} \quad (1)$$

where I_{in} is the incoming intensity *[no units]*, I_{out} is the outgoing intensity *[no units]*, c is the rate of light absorption derived multiplying the molar absorptivity *[L mol^{-1} cm^{-1}]* by the solution concentration *[mol L^{-1}]*, and x is the distance *[cm]*.

However, the calibration of a depth–reflectance relationship becomes challenging when the channel bottom is composed by sediment of different sizes, periphyton, woody debris, vegetation, senescent vegetation, artificial artefacts, etc. In fact, the composition of the channel bed can strongly affect the local reflectance of the wet areas (Legleiter et al., 2009), introducing a greater variability which should be taken into account in the depth-colour model.

Once reliable digital elevation models (DEMs) have been obtained, it is possible to detect and interpret, in a quantitative way, geomorphic changes occurring in river systems over time (e.g. Lane et al., 1994). An important component to be evaluated in DEMs is uncertainty, which can be influenced by many factors. The most decisive sources of error include survey point quality, sampling strategy, surface topographic complexity and interpolation methods (Milan et al., 2011; Panissod et al., 2009; Wheaton et al., 2010). Total uncertainty is usually derived from the classical statistical theory of errors (Taylor, 1997) where an estimation of DEM accuracy based on survey data is used as a surrogate for DEM quality (Milan et al., 2007).

This paper implements a revised approach to generate accurate and detailed Digital Terrain Models (DTMs) of a river reach by merging LiDAR data for dry areas, with water depth estimates for wet areas. The main objective consists in the evaluation of morphological patterns of change in three sub-reaches of the Brenta River as a consequence of two consecutive major floods occurred in November and December 2010. Specific aims related with the proposed approach and targeted to achieve an adequate topographic description of the river bed are: to determine physical and empirical relations between local channel depths and photo colour intensity; to identify and to filter the factors which increase uncertainty in the final DTM, in order to obtain Hybrid DTMs (HDTMs) at high resolution and low uncertainty.

2. Study area

The Brenta River is located in the South-Eastern Italian Alps, has a drainage basin of approximately 1567 km^2 and a length of 174 km. The average annual precipitation, mainly concentrated in spring and autumn, is about 1100 mm. The geology of the area is rather complex and includes limestone, dolomite, gneiss, phyllite, granite and volcanic rocks.

The study reach is 19.2 km-long and lies between Bassano Del Grappa and Piazzola sul Brenta (Fig. 1). The dominant morphologies are wandering and braided, the active channel width varies between 300 m and 800 m, and the average slope is about 0.0036 m/m. Within this study reach, three sub-reaches 1.5 km-long and 5 km apart were selected as representative of the upper- middle- and down-stream part of the study area and named according to the nearby villages: Nove, Friola and Fontaniva (Fig. 1). The upstream sub-reach (Nove) has a single straightened channel morphology with an average width of around 300 m. By contrast, Friola shows a more complex morphological pattern, with the braided channel accounting for high levels of vegetation density and an average width of 500 m. In the downstream sub-reach, called Fontaniva, the river is 800 m wide, braided and features many fluvial islands.

The Brenta river basin has suffered centuries of disturbances, mostly due to deforestation and reforestation phases. The water course has long been regulated for hydroelectric power generation and irrigation purposes and dams were built in many parts of the drainage basin, intercepting sediment from more than 40% of the drainage area. Moreover, between 1953 and 1985, gravel was intensively quarried in the main channel and, starting in the 1930s, effective erosion and torrent control works were executed in the upper basin (Bathurst et al., 2003; Conesa-Garcìa and Lenzi, 2013; Lenzi, 2006; Lenzi et al., 2003; Rigon et al., 2008, 2012; Surian et al., 2009). Human interventions, especially during the second half of the 20th century, have considerably altered the sediment budget of many Alpine rivers (Comiti, 2011; Comiti et al., 2011; Mao and Lenzi, 2007; Mao et al., 2009; Picco et al., 2013). As a result of these impacts, the average riverbed width of the Brenta has narrowed from 442 m at the beginning of the 1800s, to 196 m in 2010, and channel incision has ranged from 2 to 8 m, especially due to the effects of gravel quarrying which ended only during the 1990s (Kaless et al., 2014; Moretto et al., 2012a,b, 2013b; Surian and Cisotto, 2007). In recent times, a new adjustment phase seems to be taking place (channel widened to 215 m in 2011) as evidenced by the expanding trend of the active channel with a contemporary increase in vegetated islands over the last twenty years (Moretto et al., 2012a,

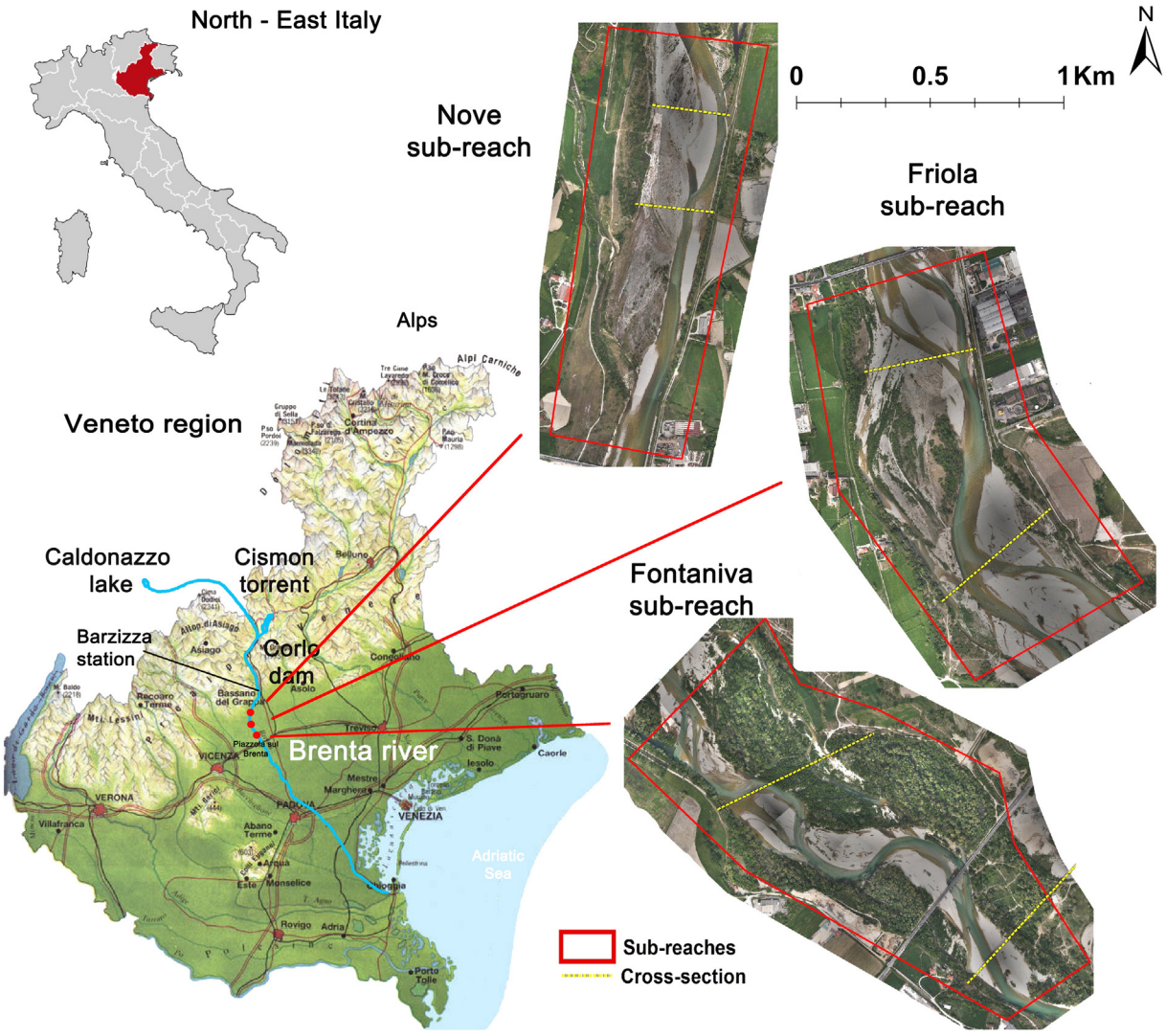

Fig. 1. General view of the Brenta river and the study sub-reaches: Nove, Friola and Fontaniva.

b, 2013b). The recent evolutionary dynamics considerably differ from those observed in the past. Since the abandonment of gravel mining activities on the river bed (1990s), there has been a partial morphological recovery, especially in the downstream sub-reach, Fontaniva. However, this trend is still unstable and not distributed along the whole study reach. In the upstream area, incision processes and a widening trend

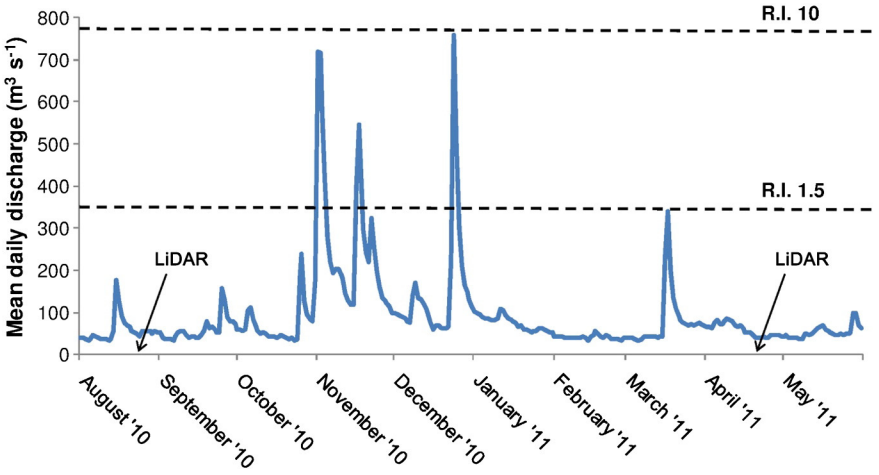

Fig. 2. Hydrograph of the study period (average daily discharges as measured at the Barzizza gauging station). Recurrence interval of the two highest flood peaks has been reached 8 years (Novembre 2010) and 10 years (Decembre 2010) respectively.

of the active channel as a result of bank erosion are still present (Moretto et al., 2012a,b, 2013b).

Two flood events have occurred between the LiDAR flights, conducted in August 2010 and on April 2011 (Fig. 2). The November 2010 flood reached a maximum average daily discharge of 720 m^3/s, with a slower drop in the water level compared to the second flood event occurred in December 2010, which reached the highest discharge of the last 10 years (maximum average daily discharge of 759 m^3/s). The recurrence intervals of these floods were estimated from the maximum annual values of the mean daily water discharge over 79 hydrological years. Among various tested probability distributions, the Gumbel distribution (OLS) demonstrated the best performance (Kolmogoroff test). Taking into account the Gumbel distribution and 90% confidence limits, it was possible to establish the flood values associated with the probability of occurrence (Kaless et al., 2011, 2014; Lenzi et al., 2010).

The first flood was caused by prolonged and heavy rainfall (300 mm) between the 31st of October and 2nd of November 2010 (Fig. 3), and featured a recurrence interval (RI) of about 8 years. The second flood, originated by intensive precipitations between the 21st and 26th of December, had a R.I. of about 10 years. Rainfall exceeded 150 mm with local maximums of 300–400 mm and the river registered (at the Barzizza station) higher hydrometric levels than the first flood event, probably due to the greater soil saturation at basin scale and, more particularly, to the fact that a major reservoir (Corlo) had already been filled by previous precipitations.

3. Material and methods

In order to create an accurate digital terrain model accounting for reliable river bed elevations, a regression model was calibrated between water depth and Red, Green and Blue (RGB) bands obtained from aerial images acquired during the LiDAR surveys. Water depth was calculated indirectly as the difference between water surface (estimated from the interpolation of selected LiDAR points; see details in Section 3.2) and channel bed elevation (measured with dGPS in the field). Hybrid Digital Terrain Models (HDTMs) were then created, by merging LiDAR (Section 3.4) points for dry areas and colour bathymetry-derived points for wet areas. Overall, three HDTMs were obtained for each year and each sub-reach (Nove, Friola and Fontaniva).

This computational process (Fig. 4) was divided into five principal steps: (A) LiDAR data and field survey, (B) dataset preparation, (C) bathymetric model determination, (D) HDTMs creation and (E) HDTMs validation. Finally, three DEMs of difference (DoDs — one for each sub-reach) were produced for each year, and the volumetric surface changes and relative uncertainty calculated (see next sections).

3.1. LiDAR data and field surveys

Two LiDAR surveys were conducted on the 23rd of August 2010 by Blom GCR Spa with an OPTECH ALTM Gemini sensor, and on the 24th of April 2011 by OGS Company with a RIEGL LMS-Q560 sensor (flying height ~ 850 m). For each LiDAR survey, a point density able to generate digital terrain models with 0.50 m resolution was commissioned. The average vertical error of the LiDAR was evaluated through dGPS points comparison on the final elevation model. The LiDAR data were taken along with a series of RGB aerial photos with 0.15 m of pixel resolution. The surveys were conducted with clear weather conditions and low hydraulic channel levels. An in-channel dGPS survey was performed, taking different depth levels in a wide range of morphological units. A total of 882 points in 2010 and 1526 points in 2011 were surveyed. Depth ranges of surveyed calibration points were between 0.20 m and 1.60 m. It is important to note that the dGPS survey was performed simultaneously to LiDAR data acquisition to avoid additional sources of errors.

Finally, two cross-sections for each sub-reach were surveyed through dGPS (average vertical error $\pm$ 0.025 m), measuring each significant topographical change and, at least, one point per metre length.

3.2. Dataset preparation

The raw LiDAR point clouds were analysed and the ground surface was identified through an automatic filtering algorithm (TerraScan, Microstation Application®). In critical areas, such as near bridges, manual checks were utilised. The aerial photos were georeferenced and corrected by applying a brightness analysis in a semi-automatic approach: the tool "reference" of TerraPhoto (Microstation application®) was used to combine aerial photos with contemporary LiDAR data and flight trajectories. The corrected photos were joined (ESRI® ArcMap 10) and the pixel size was resampled from 0.15 m to 0.50 m to minimise georeferencing errors and reduce possible strong colour variations due to light reflection, exposed sediment, periphyton, shadows and suspended load. This represents a crucial point because poor photo georeferencing may significantly increase errors due to a wrong association between water depth and colour intensity.

Wet areas were digitised through a manual photo-interpretation process. Along the edges of the digitised "wet areas", LiDAR points able to represent water surface elevation (*Zw*) were selected (to avoid points between wet and dry areas but above the water surface; e.g. on

Fig. 3. The Brenta river at Friola reach during November 2010 flood event.

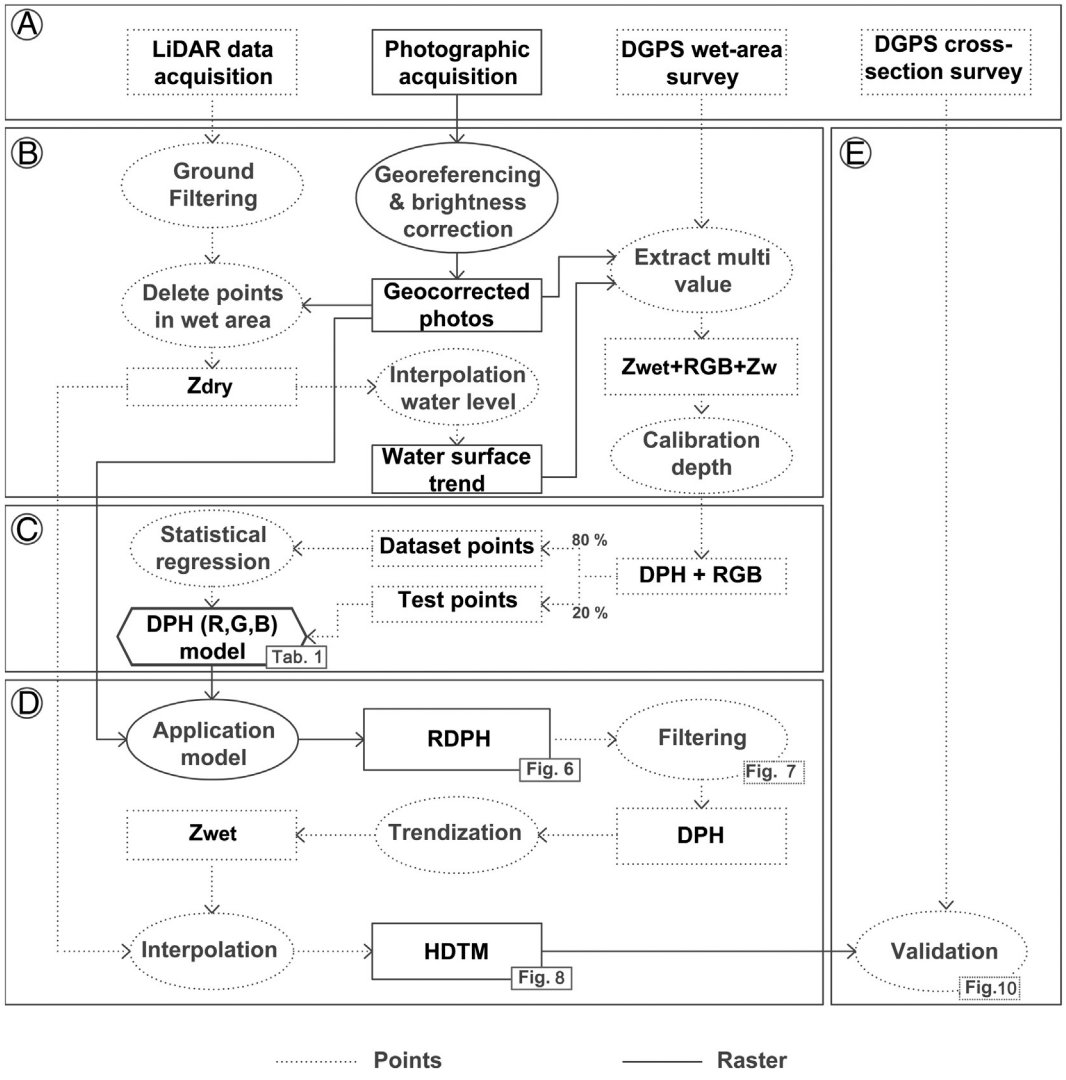

Fig. 4. HDTM creation process: (A) LiDAR data and field survey, (B) data preparation for process application, (C) bathymetric model determination, (D) hybrid DTM creation, (E) DTM validation.

a vertical bank) on average every 10 m or in correspondence of significant slope changes. These points were then used to create a water surface elevation raster (i.e. Kriging interpolation). The error of the resulting water surface was validated through 1426 water depth direct measurements taken using a graduate tape attached on the bar holding the dGPS.

Corresponding colour band intensities and *Zw* were added to the points acquired in the wet areas (dGPS wet-area survey) obtaining a shape file of points containing five fields (in addition to the spatial coordinates x and y): intensity of the three colour bands, Red (*R*), Green (*G*), Blue (*B*), elevation of the channel bed (*Zwet*), and *Zw*. Finally, channel depth was calculated as $Dph = Zw - Zwet$ [*m a.s.l.*]. These estimated water depths were validated by comparison to the water depth measured in the field. A similar method was employed by Legleiter (2013) using the difference between mean water surface elevation and bed elevation, both derived from a dGPS survey.

3.3. Determination of the best bathymetric model

Starting from the obtained dataset, water depth (estimated indirectly) was considered as dependent variable, with the three intensity colour bands (R, G and B) being independent variables. 80% of the dataset was used for calibrating the depth-colour model (calibration points) and the remaining 20% to verify the efficiency and choose the best model (test points). Physical models based on Beer Lambert law (Eq. (1)) were tested first.

A ratio-based method was employed to detect changes in depth and filter out the effect of changes in bottom albedo (e.g., Dierssen et al., 2003). Legleiter et al. (2004) and Marcus and Fonstad (2008) demonstrated that log-transformation of red-over-green band ratio linearly correlates with water depth across a wide range of substrate types:

$$DPH = \alpha + \beta_0 ln\,(R/\,G) \tag{2}$$

where *DPH* is the water depth [*m*], α and β_x are the calibration coefficient, and *R* and *G* are the intensities of the red and green bands.

An empirical linear model evaluating all the colour bands, possible interactions and square, and cubic terms, were then tested:

$$DPH = \alpha + \beta_0 R + \beta_1 G + \beta_2 B + \beta_3 RB + \beta_4 RG + \beta_5 GB + \beta_6 RGB + \beta_7 R^2 + \beta_8 G^2 + \beta_9 B^2 + \beta_{10} R^3 + \beta_{11} G^3 + \beta_{12} B^3 \tag{3}$$

where α and β_x are the calibration coefficients in the depth-colour regression. In this model, the significance of each component was tested and deleted when the adopted statistical test (explained below) resulted negative.

The statistical regressions were performed in R® environment using two methods: the "traditional regression method" based on statistical

significance testing of each variable (P-value < 0.05), and the AICc index (Burnham and Anderson, 2002).

3.4. Hybrid DTM creation and validation

The final HDTM represents a full integration between filtered LiDAR ground points and colour bathymetric points. LiDAR points were used in all dry areas and up to 0.20 m of water depth, whereas the bathymetric points were used in the remaining wet areas. The capacity of LiDAR signal to perform reliable ground points where water depth is lower than 0.20 m has been previously verified (Moretto et al., 2013a). For instance, Charlton et al. (2003) and Cavalli and Tarolli (2011) have reported that LiDAR pulse is able to penetrate shallow water when the laser signal is not distorted. The unreliability of colour bathymetry in representing water depths lower than 0.20 m when there is a strong colour variation at the cannel bottom (periphyton, exposed pebbles, woody debris, etc.), has been verified in the field. In these conditions, remarkable errors may be introduced (> ± 0.20 m) in depth estimations (Legleiter et al., 2009).

The best bathymetric model for each year was therefore applied to the wet areas starting from 0.20 m of water depth down (measured from the water surface elevation raster) on the georeferenced images, to determine the "Raw Channel Depth Raster" (RDPH). The RDPH was then transformed into points (4 points/m^2) and filtered, as explained below, in order to delete uncorrected points, mainly due to sunlight reflection, turbulence, strong periphyton presence, and elements (wood or sediment) above the water surface. According to this approach, the filtered depth (DPH) model was finally obtained.

To filter out possible incorrect points, a method based on the analysis of slope changes in neighbouring cells was adopted. Changes of local slope calculated among neighbouring cells were analysed through a semi-automatic method which uses a "curvature raster" (Curvature tool - ESRI® ArcMap 10 - Moore et al., 1991), obtaining a value of curvature (slope derivative) for each cell. The curvature tool calculates for each cell the second derivate value of the input surface (RDPH) on a cell-by-cell basis (3 × 3 moving window). For ranges of curvature >700 or <−600, cells were considered incorrect outliers and consequently eliminated. This range was derived from dGPS survey analysis and joined with direct observations over the estimated wet raster, on which no changes in elevation greater than ± 0.60 m were present within a horizontal distance of <0.50 m. In other words, all areas with an unreal slope variation (derived by curvature calculation) outside the proposed curvature range were removed. In addition, non-surface points (outliers; <5 % of total points distribution) were also deleted.

After the filtering of points, the "water depth model" (*DPH* — water depth model) was finally obtained. For each point, the corresponding *Zw* [*m a.s.l.*] was subtracted to acquire the estimated river bed elevation ($Zwet = Zw - DPH = [m\ a.s.l]$). Hybrid DTMs (HDTM) were built up with a natural neighbour interpolator, integrating Zdry points (from LiDAR) in the dry areas and in the first wet layer (0–0.20 m) and Zwet points (from colour bathymetry) in the remaining wet areas.

Finally, the HDTM models were validated by using dGPS cross-sectional surveys. The error of each "control point" was derived considering the difference between elevation of the HDTM and corresponding elevation of the dGPS control points.

The accuracy of HDTMs was estimated separately for wet and dry areas, also taking into account the dGPS error (available from the instrument for each point). The average uncertainty for both wet and dry areas was calculated averaging the error derived by each dGPS control point available for the correspondent dry or wet area. The total average uncertainty was calculated by weighting dry and wet uncertainties with the correspondent surfaces. The error for each water layer (every 0.20 m of depth) was also calculated.

3.5. Analysis of morphological changes

The high-resolution HDTMs allowed the exploration of the morphological effects of the flood events occurred between our considered surveys.

The Geomorphic Change Detection 5.0 (GCD) software developed by Wheaton et al., 2010 (http://gcd.joewheaton.org) was used to perform reliable DEMs of Difference (DoDs). Elevation uncertainty associated with the DoDs was calculated in Matlab environment (Fuzzy Logic application) using an "ad hoc" FIS file and considering slope, point density and bathymetric points quality as input variables. Slope and point density categorical limits (low, medium, high) were chosen taking into account values available in the literature (Wheaton et al., 2010) and local environment. Bathymetric points quality was used to delete erroneous cells from the HDTMs in the final erosion–deposition volume computation (see Delai et al., 2014 for further details).

Table 1
Depth-colour model estimated by traditional and AICc method.

Model	Depth-colour model estimated by traditional method	p-value	r^2	Error (m)
Beer Lamb. 2010	$DPH = -0.119 + 2.725\ ln\ (R/G)$	2.2×10^{-16}	0.34	±0.27
Beer Lamb. 2011	$DPH = -0.73 + 2.043\ ln\ (R/G)$	2.2×10^{-16}	0.25	±0.20
Empirical 2010	$DPH = 5.31 + 0.07513\ R - 0.1869\ G - 0.01475\ B - 0.0004582\ RB + 0.001056\ G^2 + 0.0003352\ B^2 - 0.000002142\ G^3$	2.2×10^{-16}	0.46	±0.26
Empirical 2011	$DPH = -0.607 + 0.03508\ R - 0.06376\ G - 0.1377\ B + 0.002257\ RG - 0.001096\ RB + 0.002303\ GB - 0.0007273\ R^2 - 0.002956\ G^2 + 0.0009993\ B^2 + 0.000002837\ G^3 - 0.00000685\ B^3$	2.2×10^{-16}	0.38	±0.19

Model	Depth-colour model estimated by AICc method	p-value	r^2	Error (m)
Beer Lamb. 2010	$DPH = -0.119 + 2.725\ ln\ (R/G)$	n. a.	n. a.	±0.27
Beer Lamb. 2011	$DPH = -0.73 + 2.043\ ln\ (R/G)$	n. a.	n. a.	±0.20
Empirical 2010	$DPH = 5.28 + 0.0000003527\ R + 0.001189\ G - 0.02082\ B + 265\ BR - 122.316\ BG + 0.073\ RGB - 0.0008215\ R^2 - 0.000002506\ G^2 + 0.0005809\ B^2 + 10\ R^3 + 0.09595\ G^3 - 0.2026\ B^3$	n. a.	n. a.	±0.26
Empirical 2011	$DPH = -0.607 + 0.03508\ R - 0.06376\ G - 0.1377\ B + 0.002257\ RG - 0.001096\ RB + 0.002303\ GB - 0.0007273\ R^2 - 0.002956\ G^2 + 0.0009993\ B^2 + 0.000002837\ G^3 - 0.00000685\ B^3$	n. a.	n. a.	±0.19

Where *DPH* is the water depth [*m*], *ln (R/G)* are the colour bands arranged according to the Beer Lambert law. R, G and B are respectively the red, green and blue colour bands of the aerial photos. "P-value" and "square r" are parameters not available (*n.a.*) for AICc approach that has a complete different method of regression (Burnham and Anderson, 2002). The error (m) is derived from the model application on the 20 % of test points independents from the model calibration process with both statistical methods presented.

Geomorphic changes in the study reaches were finally calculated, similarly to Wheaton et al. (2010), by using a spatially variable uncertainty thresholded at 95% C.I. and the Bayesian updating method which accounts for spatial coherent erosion and deposition units (5 × 5 mobile windows).

A HDTMs comparison aimed at analysing the dynamics of the bed forms (riffle–pool) as a consequence of flood events and natural and artificial "constrictions", was subsequently performed in order to integrate erosion–deposition patterns analysis.

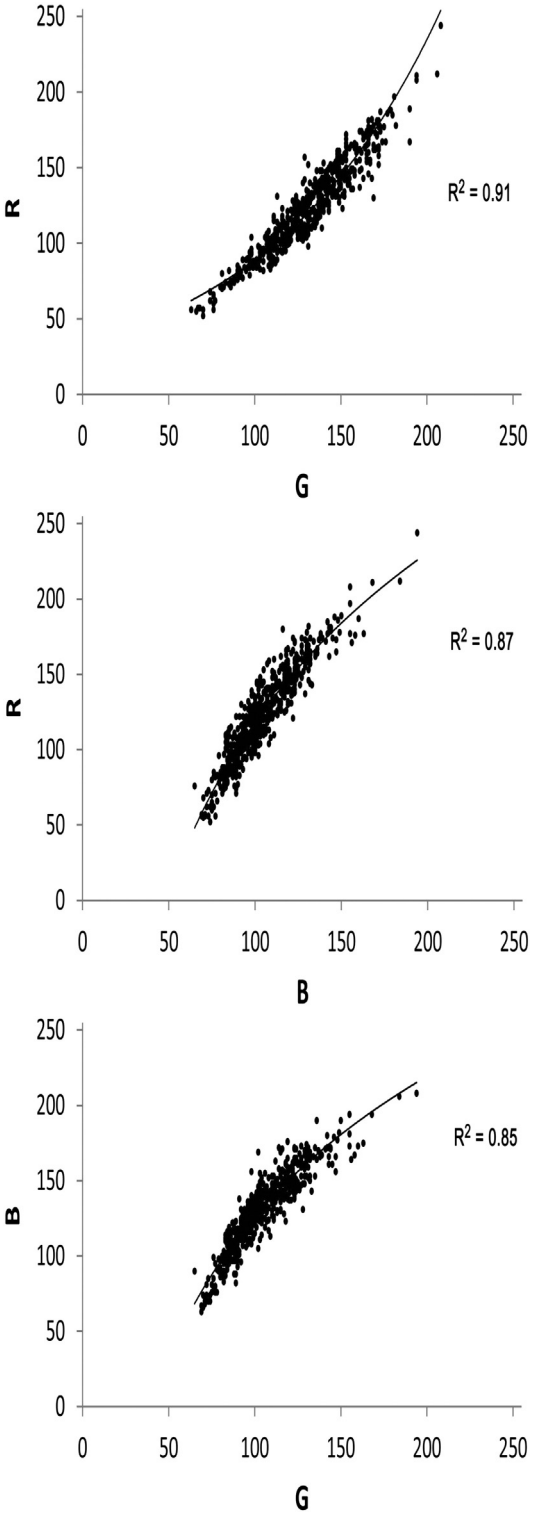

Fig. 5. Correlation between Red, Green and Blue colour bands.

Canopy surface models (CSM), derived from the difference between digital surface models (DSM) and DTMs, were produced to identify natural (fluvial islands) and artificial (embankments and bridges) vertical construction in the analysed sub-reaches. In addition to the bathymetric rasters, three water depth classes (0–0.50 m; 0.50–1 m and > 1 m) were applied to identify different bed forms.

4. Results

4.1. Colour bathymetry models

To understand the average and the range of channel depths, the average, standard deviation and maximum depth of 2010 and 2011 wet channels were estimated before calibrating the regression model. 2010 was characterised by an average depth of 0.53 m, a standard deviation of 0.34 m and a maximum known depth of 1.62 m. 2011 had a greater average depth than 2010 equal to 0.63 m, a standard deviation of 0.28 m and a maximum known depth of 2.30 m.

The indirect water depth estimation was validated thanks to 1426 direct measurements of water depth taken using a graduate tape attached on the bar holding the dGPS, and an average error of ±0.15 m was recognised. This error may be due to LiDAR vertical error (used to interpolate the water surface), water turbulence around the graduated bar, and by natural roughness of the bed surface (mainly cobbled; D_{84} = 64–87 mm, Moretto et al., 2012b).

The search for the best depth-colour model started from the composed datasets by testing a physical model, based on the Beer Lambert law (Eq. (2)) for each year (2010 and 2011) and with the two introduced statistical regression methods (traditional regression and AICc index; Section 3.3).

The application of the traditional regression method and the AICc index produced the same depth colour model for 2010 (see Beer Lambert 2010 equations on Table 1).

This model has a statistically significant p-value ≪0.05, and an average error derived from the test points of ±0.27 m. A similar result was obtained for the 2011 model; also in this case the two statistical regression methods have produced the same result (see Beer Lambert 2011 equations on Table 1). This model has a statistically significant p-value ≪0.05, and an average error derived from the test points of ±0.20 m.

The *depth-colour (RGB)* statistical regressions performed with the empirical model and using the two different approaches allowed two bathymetric models to be obtained for each year (2010 and 2011 empirical models — Table 1).

The average errors detected in the two models by comparing the test points are equal to ±0.26 m. Negligible differences (0.003 m of difference of average error) between the considered models (Table 1 — Empirical 2010 equations), traditional and AICc methods, were estimated. Therefore, the model resulting from the traditional method (see empirical 2010 equation in Table 1) was preferred because of its simpler structure with fewer factors if compared to the AICc model. In these models (Table 1), *DPH* is the estimated water depth [*m*] and R, G and B are the red, green and blue bands, respectively.

If 2011 is considered, the two different methodologies (traditional and AICc index) of statistical regression, generated the same equations as showed in Table 1 (Empirical 2011 equations). The estimated depth average error of 2011 resulting from the test points, accounts for ± 0.19 m.

Both physical and empirical models proved to be statistically significant (p-value ≪0.05), but the empirical models seem to have more predictive capacity than the physical approaches (see r^2 on table 1). In addition, all three colour bands significantly contribute to depth estimation, therefore the presence of interactions between colour bands (as reported in Fig. 5) should be taken into consideration.

Fig. 6 shows one of the outputs deriving from the model application (Table 1 — Empirical 2011 equations) in Friola sub-reach. It appears that

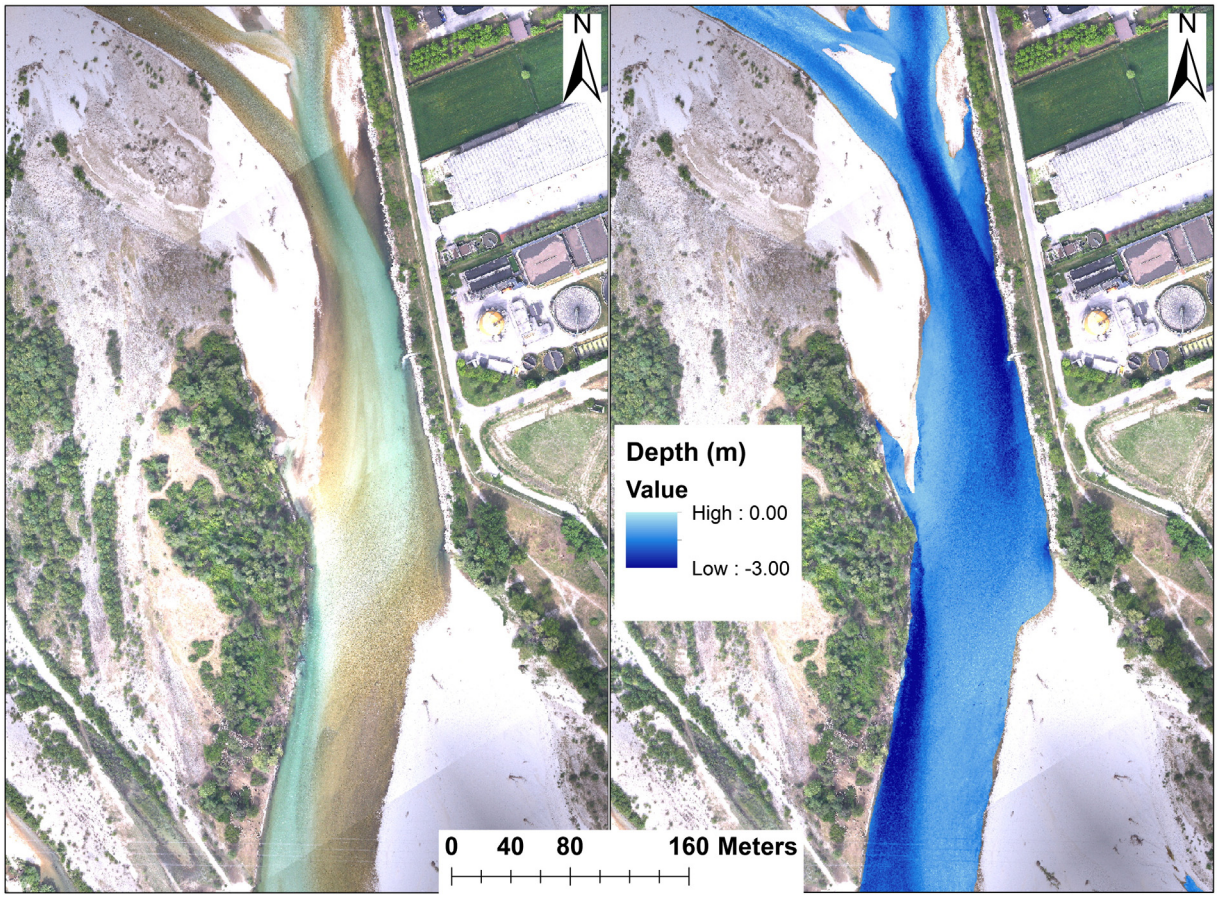

Fig. 6. Model application (8) at Friola sub-reach (2011). The brown zones on the left side are due to the presence of *periphyton* at the channel bottom.

depth variations are generally respected, and variations in colour tone due to the presence of periphyton in the channel bed do not seem to strongly influence the estimation of water depth. In this sub-reach, the maximum estimated water depth exceeds 2 m.

4.2. HDTM production and validation

The presented filters, used to delete raw depth points not belonging to water surface (due to model application on altered pixel colour value) were applied on RDPH models.

A cross-sections comparison of 2011 raw HDTM and the HDTM derived from the profiles of Friola wet areas is shown in Fig. 7. The sections highlight the goodness of the applied filters. Also, the principal sources of error such as water turbulence, light reflections, suspended load, strong periphyton and exposed sediments appears to have been filtered by the curvature calculation.

The percentage of filtered depth points in Nove, Friola and Fontaniva on 2010 wet areas were 3.39 %, 4.88 %, and 0.37 %, respectively. Instead, the percentage of filtered depth points in Nove, Friola and Fontaniva on 2011 wet areas were 4.32 %, 2.60 %, and 18.11 %, respectively. In

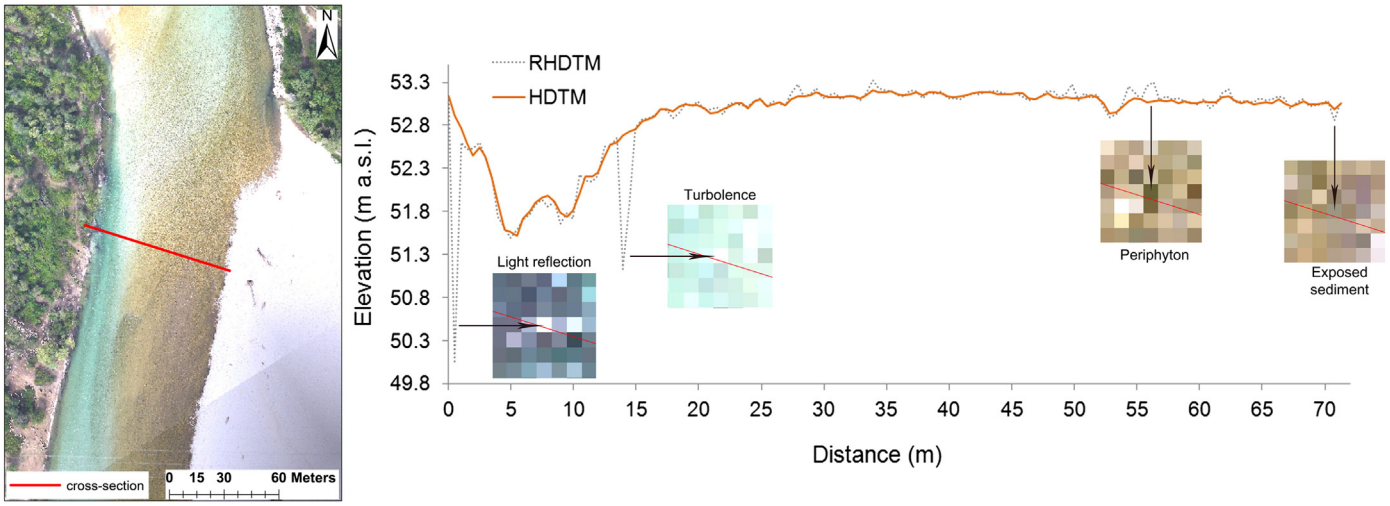

Fig. 7. Example of filtering process in a cross-section of Friola sub-reach (2011).

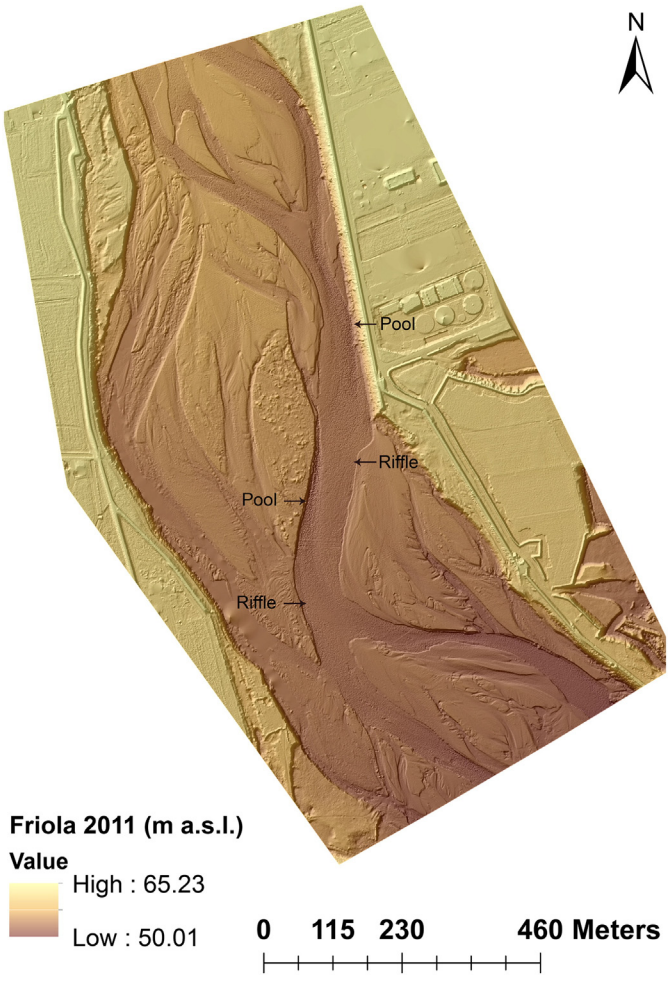

Fig. 8. Hybrid Digital Terrain Model (HDTM) of Friola sub-reach, 2011, cell size 0.50 × 0.50 m.

Fontaniva, more than 90,000 of the 499,596 depth raw points had to be filtered out. This was the case in which more points needed filtering due to the presence of marked shadows generated by dense riparian vegetation growing on banks (see Fig. 1).

After filtering raw depth points, dry areas and the first 0.20 m of water depths were integrated using the LiDAR flight. LiDAR point clouds (excluding wet areas) featured an average density of 2.07 points/m^2 for 2010 and 2.64 points/m^2 for 2011. The final HDTMs, three for 2010 and three for 2011 (Nove, Friola and Fontaniva sub-reaches) were generated using a 0.50 × 0.50 m cell size. Fig. 8 shows the HDTM obtained for Friola 2011. It is worth noticing the good representation of bed-forms such as riffles and pools within the wet channels.

Data validation (Table 2) was performed separately for both wet and dry areas, obtaining average uncertainty values (by field survey comparison) for each HDTM including dGPS, LiDAR and DPH estimated errors. Average uncertainty associated to wet areas accounts from a minimum of ± 0.19 m (Friola in 2011) to a maximum of ± 0.26 m (Nove and Fontaniva in 2010 and 2011), whereas in dry areas the average uncertainty ranges from a minimum of ± 0.14 m (Nove in 2010) to a maximum of ± 0.26 m (Fontaniva in 2010). The chosen colour bathymetric models (empirical depth-RGB) generated similar error levels, on dry and wet areas, for both 2010 and 2011. Moreover, the average weighted uncertainty was calculated in the final HDTMs, ranging from ± 0.16 m, for Nove 2010–2011 and Friola 2011, to ± 0.26 m in Fontaniva reach in 2010.

If the errors associated with the HDTMs on wet areas are taken into consideration, the reliability of wet areas estimates in the HDTMs can be appreciated (Fig. 9). The percentage of control points within ± 0.30 m of error is equal to 75 % and 84 % for 2010 and 2011, respectively. Fig. 9 shows that the higher errors correspond to the maximum water depth and are up to 1 m and 1.20 m for 2010 and 2011, respectively. The distribution of average errors, standard deviations and their aerial extent on the entire wet areas among different water depths are showed in Table 3.

Fig. 10 reports an example of a comparison of three cross-sections for 2011, obtained with three different types of data (dGPS survey, LiDAR, and HDTM). The reference section was surveyed using a dGPS and ground points feature an average error of about 0.025 m.

On the right hand side of Fig. 10 (zoom to the wet areas), we can appreciate a comparison between dGPS and LiDAR profiles: the ability of LiDAR signal to penetrate wet areas up to 0.25–0.30 m is confirmed. On the other hand, the use of LiDAR-derived water depth in channel areas deeper than 0.25–0.30 m can lead to underestimation of water depth, and a consequent overestimation of calculated DoD volumes, as showed in Table 1. These volumes were derived as a subtraction between HDTMs and DTMs (derived entirely from LiDAR). The minimum volume of 397,470 m^3 is registered at Friola, whereas the maximum of 4,743,783 m^3 at Fontaniva. Instead, comparing dGPS and HDTM profiles, it appears that, overall, ground points are well replicated except for some small areas lower than the dGPS profiles (Fig. 10). This may be due, in part, to the presence of large boulders in the water channel that have altered the resulting cross-sections between precise dGPS measurements and those derived from a mediated profile by HDTM cells of 0.50 × 0.50 m. The maximum registered depth is well replicated

Table 2
Estimated uncertainty for HDTM and DoD models.

		NOVE		FRIOLA		FONTANIVA	
		2010	2011	2010	2011	2010	2011
HDTM area	(m^2)	566,916	566,916	836,967	836,967	627,049	627,049
Wet area	(m^2)	95,607	89,613	107,758	135,227	75,616	113,974
Wet area/HDTM area		0.17	0.16	0.13	0.16	0.12	0.18
N° dGPS point for test DTM_{BTH}		192	408	279	821	204	283
Average unc. DTM_{BTH} & dGPS	(m)	0.26	0.26	0.25	0.19	0.26	0.26
N° dGPS point for test DTM_{LD}		72	132	98	155	53	64
Average unc. DTM_{LD} & dGPS	(m)	0.14	0.15	0.24	0.15	0.26	0.16
TOTAL average uncertainty	(m)	0.16	0.17	0.24	0.16	0.26	0.18
DoD (HDTM Vs. $DTM_{Full\ LiDAR}$)	(m^3)	917,559	529,812	1,206,848	397,470	4,386,814	4,743,783
DoD ($HDTM_{2011}$ Vs. $HDTM_{2010}$)		Er.	Dep.	Er.	Dep.	Er.	Dep.
	(m^3)	122,498	18,416	177,951	95,030	158,359	113,127

DTM_{BTH}: Part of Digital Elevation Model derived by Bathymetry; DTM_{LD}: Part of Digital Elevation Model derived by Light Detection and Ranging; dGPS: Differential Global Positioning System; $DTM_{BTH\ or\ LD}$ & dGPS: sum of DTM and dGPS error; $DTM_{Full\ LiDAR}$: DTM totally derived from LiDAR; Er.: Erosion; Dep.: Deposition.

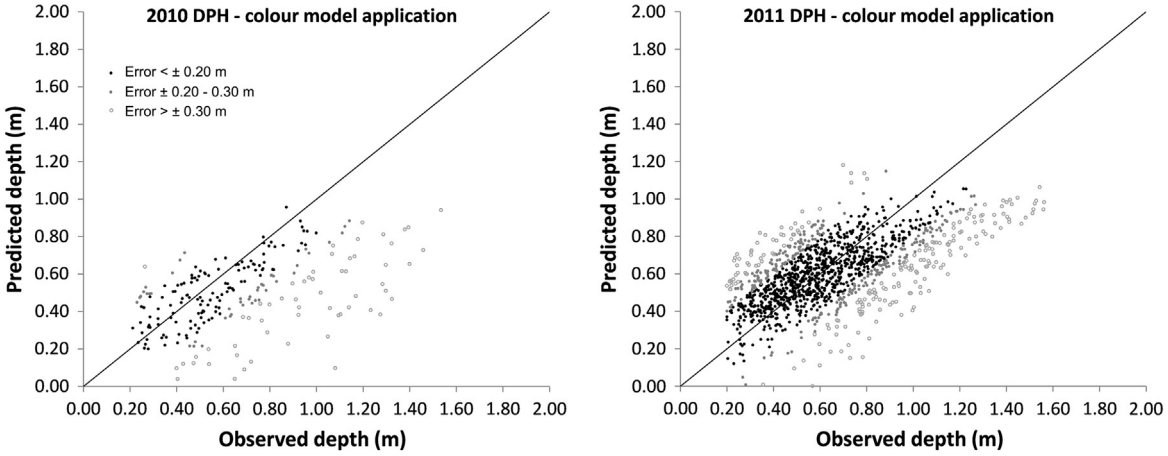

Fig. 9. Observed depth versus predicted depth classified by three level of errors:<±0.20 m;±0.20–0.30 m and > ±0.30 m.

by colour bathymetry (comparing dGPS cross sections) and reaches 2 m as showed in Fig. 10c.

4.3. Morphological change detection

The effects of November and December 2010 floods on Nove sub-reach can be appreciated in Fig. 11a. Overall, erosion exceeds sedimentation (122,498 vs. 18,416 m^3; Table 2), and erosion consistently occurs along the main channel in the whole reach with a thickness of >0.20 m.

Considering Friola sub-reach, the volumes of erosion and deposition appear to be more similar than Nove, ranging around 177,951 m^3 and 95,030 m^3, respectively (Table 2). Similarly, erosion occurs consistently along the main channels with a thickness of >0.20–0.50 m. In Friola, erosion of bars leading to lateral migration of the main channel can be depicted (Fig. 11b).

In the lowermost sub-reach (Fontaniva) deposition and erosion are volumetrically comparable, being around 158,359 m^3 and 113,127 m^3, respectively (Table 2). The erosion process is not continuous along the main channels as for Nove and Friola, but shows a more complex pattern. Two different portions of the reach can be identified, being the upper one dominated by deposition, whereas the lower by predominant erosion.

Fig. 12 shows the CSMs with the location of pools (e.g. P1, P2) on wet areas of Nove, Friola and Fontaniva sub-reaches in 2010 and 2011. Pools are identified as dark areas, i.e. the zones with the higher water depth if compared to the riffles. It is worth noticing how the main channel appears to have increased its sinuosity on the reaches where fewer lateral constrictions are present. Nove sub-reach is the most laterally constrained due to artificial left embankments featuring also the highest incision degree, and the main channel appears to have maintained the same sinuosity.

Considering bed-forms after floods, pools appear to have increased in length. This is particularly evident in Friola sub-reach (pool P3 and P4, 2011) and Fontaniva (pool P4, 2011). The embankments and fluvial islands appear to have played an important role in bed-form dynamics during floods. Indeed, pools in each 2011 sub-reach are located mainly at the side of the wet area with a more compact lateral surface with embankments and/or vegetated bars. On the other hand, riffles are mainly located where no significant "constrictions" were present on either side of the wet areas.

5. Discussion

5.1. Analysis of the proposed method for geomorphic change detection

The proposed method is a revised procedure for the production of high resolution DTMs on gravel-bed rivers, integrating LiDAR points

Table 3
Error analysis of depth-colour models at different water stages for 2010 and 2011. The average error and standard deviation have been weighted with the correspondence inference area.

	Depth	Surface covered		DPH (R, G, B)		Survey method
	(m)	(ha)	%	error (m)	St. dev. (m)	
2010)						
	0.00–0.19	9.23	33.1	0.26	0.22	LiDAR
	0.20–0.39	6.88	27.7	0.26	0.24	Colour bathymetry
	0.40–0.59	6.29	22.6	0.21	0.20	
	0.60–0.79	4.26	15.3	0.22	0.18	
	0.80–0.99	0.98	3.5	0.26	0.15	
	1.00–1.19	0.29	0.8	0.51	0.21	
	>1.20	0.03	0.1	0.69	0.14	
	TOTAL	**27.90**	**100**	**0.25**	**0.21**	
2011)						
	0.00–0.19	0.17	0.5	0.27	0.11	LiDAR
	0.20–0.39	2.32	6.9	0.18	0.11	Colour bathymetry
	0.40–0.59	8.46	25.0	0.13	0.11	
	0.60–0.79	9.40	27.7	0.14	0.13	
	0.80–0.99	6.77	20.0	0.24	0.19	
	1.00–1.19	3.14	9.3	0.32	0.19	
	1.20–1.39	1.90	5.6	0.40	0.13	
	>1.40	1.72	5.1	0.56	0.10	
	TOTAL	**33.89**	**100**	**0.21**	**0.14**	

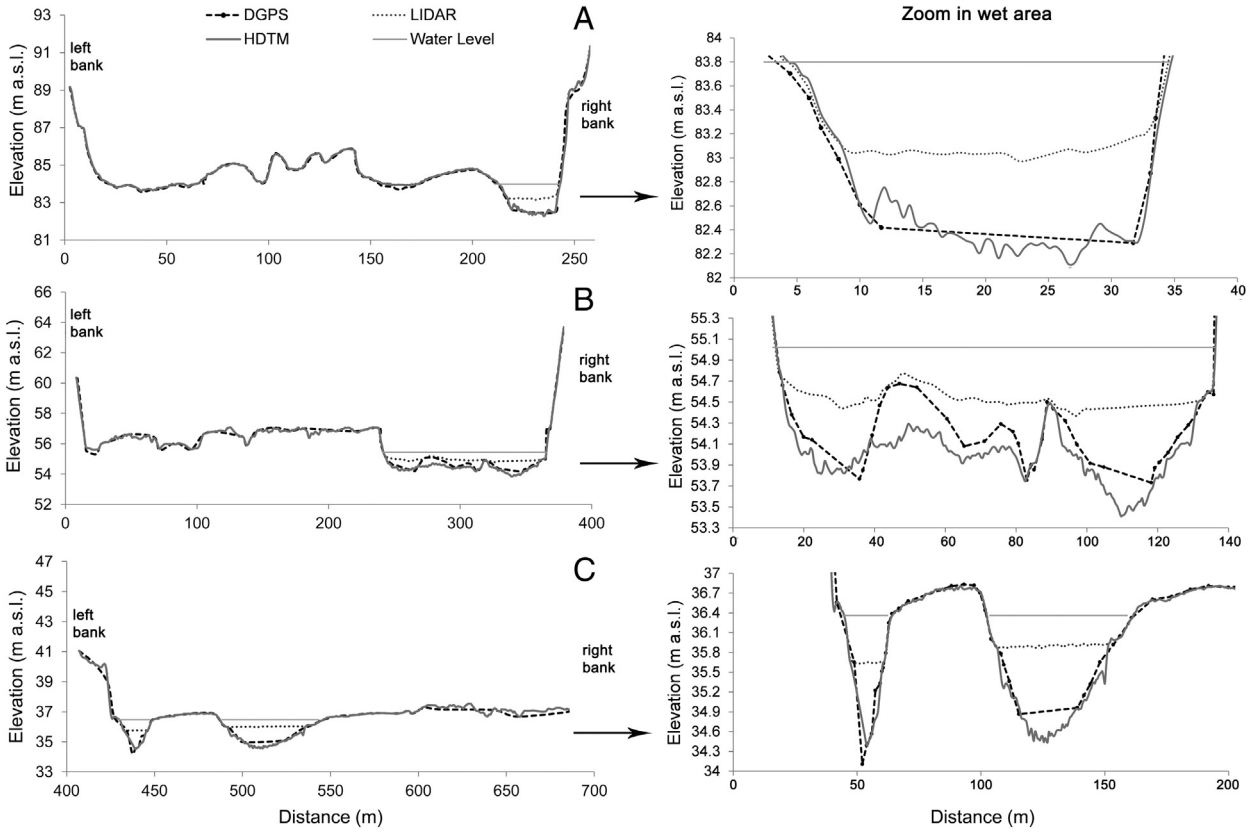

Fig. 10. Cross-section comparison on the left hand side between dGPS, HDTM and LiDAR surveys of Nove (a), Friola (b) and Fontaniva (c) 2011. Cross-section zoom in wet area on the right hand side.

with filtered bathymetric points estimated through a regression model implemented on wet areas.

The bathymetric points can be derived from a physical and empirical relationship between water depth and RGB bands of aerial images taken concurrently with LiDAR data.

The model calibration requires a dGPS survey of water level, without direct water depth measurements. It is crucial to acquire dGPS points nearly contemporary to LiDAR and aerial images, as already pointed out by Legleiter (2011). In fact, the calibration of the model does not need direct field surveys of water depth because this is indirectly estimated. Depth estimation entailed the subtraction of water level raster (water surface) from corresponding dGPS elevation points (bottom surface) of the channel bed (Zwet). This method is an effective approach for indirect estimation of water depth and similar to the technique used by Carbonneau et al. (2006).

Indirectly estimated depths (see Section 3.2), together with corresponding RGB values, are the values needed for the statistical calibration of the regression models. The statistical analysis showed that all

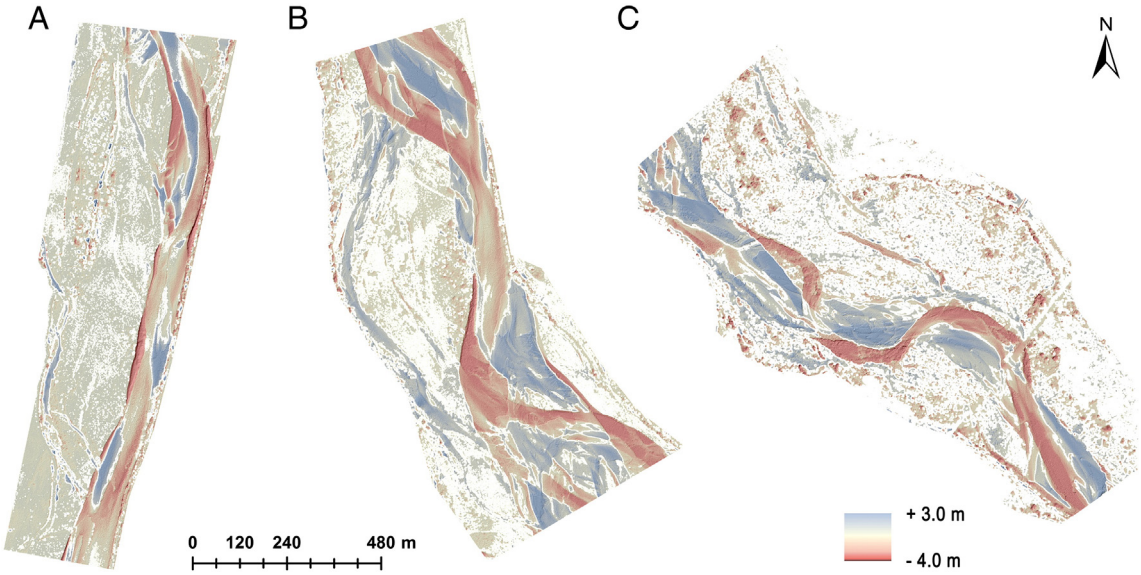

Fig. 11. Difference of DEMs (DoD) of Nove, Friola and Fontaniva sub-reaches.

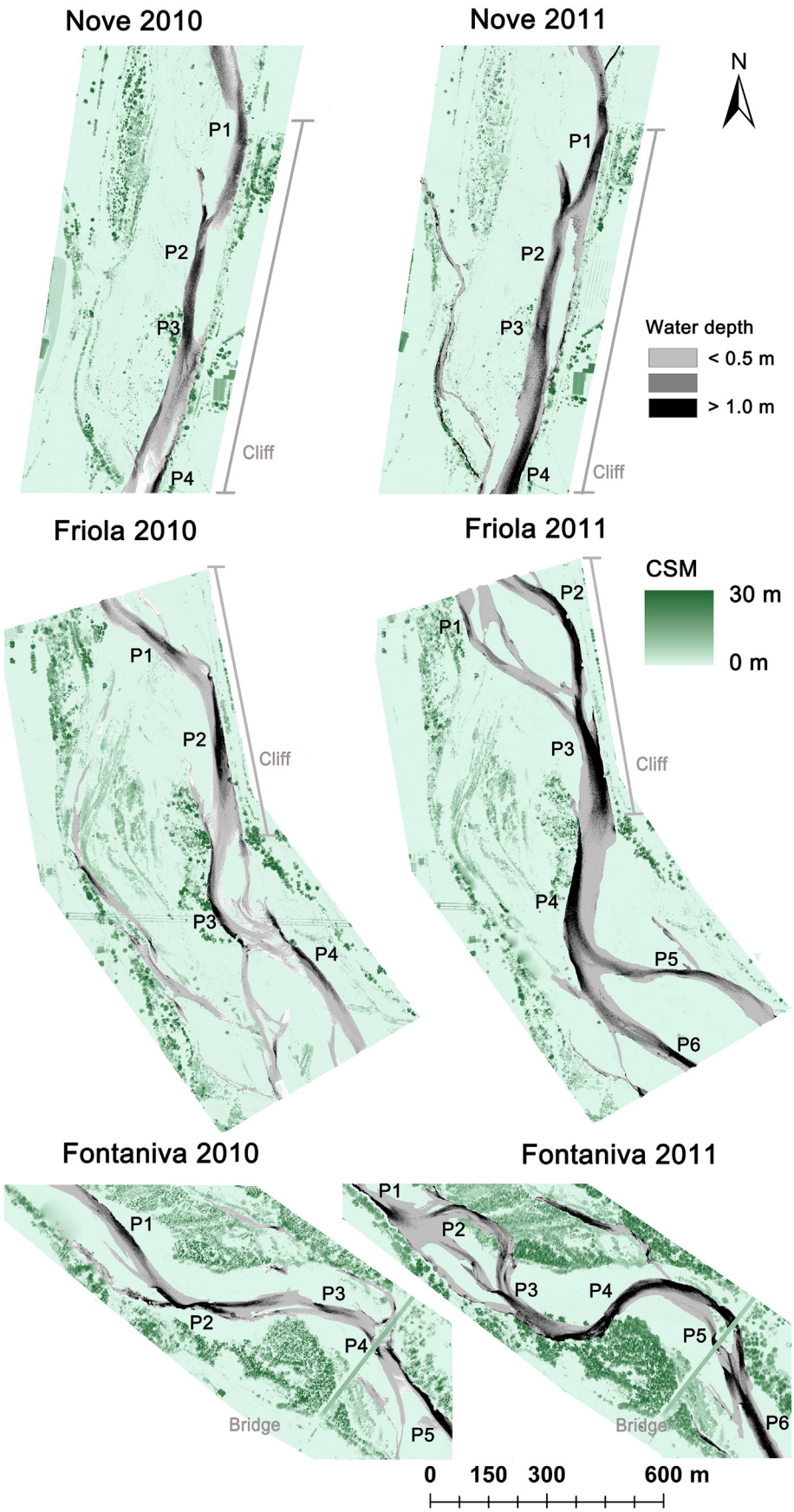

Fig. 12. Canopy surface models (CSM) with pools individuation (P1, P2, etc.) through bathymetric raster on wet area in Nove, Friola and Fontaniva sub-reaches 2010 and 2011.

three bands (R, G, B) and also some of the other additional factors (interactions among bands and square and cubic terms) were significant (p-value ≪ 0.05) to predict water depth. This statistical significance was also confirmed by two different statistical regression methods (verification of p-value and AICc index). The "ad hoc" calibration for each study year was necessary because of the different water stage during LiDAR survey.

This study has demonstrated that in a wet area with complex and heterogeneous channel bed, and with different colours on channel bottom (due to the presence of periphyton), the tested depth-colour physical models does not perform as well as the empirical models. Indeed, the presence of periphyton on the channel bed can be claimed as one of the error sources (i.e. low r^2) in assessing water depth, as previously suggested by similar studies (e.g. Carbonneau et al., 2006; Legleiter et al., 2011; Williams et al., 2014). Despite a lower r^2, the final validation of the elevation models (shown in Fig. 10 and Table 2) has demonstrated a bathymetric uncertainty comparable to LiDAR data in dry area.

Table 3 shows that the optimal application range of the estimated bathymetric models is between 0.20 m and 1–1.20 m for 2010 and 2011, respectively. Even though the best application range of estimated depths is lower than 1.20 m, local good estimations of wet channel up to 2 m of water depth were observed in cross section comparisons (Fig. 10c). The ability of LiDAR signal to allow a reliable estimate in the first 20 cm of water column was confirmed by dGPS and LiDAR cross-section comparisons (Fig. 10) as well as in Moretto et al. (2013a). Smith et al. (2012) and Smith and Vericat (2013) report that a further source of error could be due to laser refraction of LiDAR signal when penetrating into water. Although this error cannot be excluded in this study, it can be considered lower than other sources, because airborne LiDAR signal has a near-vertical angle of incidence, thus presenting a minimum level of refraction. Different errors at the same depth (Table 3) between the two depth-colour models (one for each year) are likely due to the different number of calibration points among different water depth ranges and different image luminosity conditions. In Moretto et al. (2013a), the average error every 0.20 m of water depth associated with the number of calibration points was calculated. A similar bathymetric approach was applied, but lower errors (<±0.26 m) were assessed up to 1.60 m likely due to a larger amount of calibration points available. In this work, a calibration dataset as wide as the one used for the Tagliamento River in Moretto et al. (2013a) was unfortunately not available. Therefore, a preliminary analysis aimed at assessing both percentage of present wet surface in the study area and range of depths, is required. In this way, a minimum number of calibration points for each water depth range can be decided, allowing an acceptable error for most part of the wet areas.

Despite the possible sources of errors, the proposed approach allowed to generate elevation models with a vertical error lower than ± 0.22 m for 95.6 % of the 2010 wet area and lower than ± 0.26 m for 99.1 % of the same surface. For 2011, we obtained vertical errors lower than ± 0.24 m for 80.0 % and lower than ± 0.32 m for 89.3 % of the wet area, respectively. Hydraulic conditions at the time of LiDAR survey were not exactly the same in 2010 and 2011 (see Section 4.1), and the number of calibration points can play a significant role especially in a very variable fluvial environment.

The importance of using a bathymetric method for evaluating erosion–deposition patterns by applying numerical models or developing sediment budgets is showed in Table 2 where the loss of volume without applying colour bathymetry is reported.

In Fig. 7, different types of errors were identified in the raw HDTM: light reflection, water turbulence, periphyton and exposed sediment (sources of errors highlighted also by Legleiter et al., 2009). Light reflection and water turbulence (white pixels) produce strongly negative depth estimates and substantially different (about 1–2 m) values from adjacent pixels not affected by these problems. Exposed or nearly exposed periphyton (green and brown pixels) and exposed sediment (grey pixels) produce an underestimation or overestimation of water depth (about ± 0.40–0.60 m of difference with respect to the adjacent pixels). The correction method which involves the use of a filter based on curvature and consequent removal of outliers (points with errors exceeding 95 % of confidence interval), has provided to work well as depicted in Fig. 7. In this way the quality of the final HDTMs have been clearly improved.

Shadows represent a disturbance factor difficult to correct and remove because they tend to cause an overestimation of channel depth. However, their presence was minimal in the study sites, thanks to image acquisition carried out around midday. The model tends to underestimate water depth where this exceeds 1–1.10 m. This is partially due to the low availability of calibration points (for safety reasons) in the deepest areas of the water channel. Furthermore, in deeper water, depth estimates through aerial images become less reliable due to the increase in saturation of the radiance signal (Legleiter, 2013).

The main topographical variations, as showed in the comparison between HDTMs and dGPS cross-sections (Fig. 10), result as being faithfully reproduced, except for the thalweg, which was difficult to detect with a dGPS survey. Consequently, the resulting HDTMs can be considered as a satisfactory topographical representation (considering the resolution of the final elevation models) for the homogeneous study of morphological variations.

5.2. Geomorphic changes after 2010 floods

The morphological evolution of the Brenta River over the last 30 years has been strongly influenced by human impacts and flood events (Moretto et al., 2013b). Lateral annual adjustment is directly correlated with the mean annual peak discharge (Moretto et al., 2012a, 2013b), thus a higher flood magnitude generally corresponds to greater active channel widening. Substantial increases in channel width and reductions of riparian vegetation occur due to flood events with an RI higher than 5 years, as already highlighted by other studies on fluvial environments similar to the Brenta River (e.g. Bertoldi et al., 2009; Comiti et al., 2011; Kaless et al., 2014; Picco et al., 2012a,b, 2014). The flood events of November–December 2010 in the Brenta River (RI = 8–10 years) have caused an increase of the active channel average width of about 10 % (from 196 m to 215 m) with a consequent removal of 10 ha of riparian vegetation in the study reach (for more detailed information see Moretto et al., 2012a,b). It is worth pointing out that the predominance of erosion processes, with a consequence negative balance between erosion and deposition, decreases from the upper to the lower sub-reach and is equal to −104,082 m^3, −82,921 m^3 and −45,232 m^3, respectively.

It is interesting to note the presence of a continuous eroded layer along the main channels (0.20–0.50 m of depth) along Nove and Friola sub-reaches. Instead, in Fontaniva sub-reach the upper part features predominant deposition dynamics, whereas erosion seems to dominate in the lower part.

The analysed flood events seem to have generated riffle–pool migrations on unconfined sections (e.g. P1 on Friola and Fontaniva 2010), while a pool enlargement occurred beside an artificial lateral constriction (e.g. P4 on Nove and P3–P4 on Friola 2011). The location and geometry of the new bed forms seem to be related to the natural (vegetated bar) and anthropic (embankments and bridges) constrictions. If pools are compared from 2010 to 2011, it appears that after a severe flood event, they are generally longer and migrations are more concentrated on reaches partially or totally confined (Fig. 12).

The different behaviour of the three sub-reaches seems to be attributable to their different morphological characteristics (natural and imposed) and the availability of sediment from the upstream reach (Moretto et al., 2012a,b, 2013b). The first sub-reach (Nove) is the most affected by erosion processes (Moretto et al., 2012a). The conditions of Nove sub-reach can be summarised as follows: i) past and present heavy incision of the active channel with modifications in section shape and from the river basin; ii) very little sediment supply from

upstream reaches; iii) almost total absence of vegetation on the floodplain; iv) increase of local slope.

The second sub-reach, Friola, has a lower slope and is less laterally constrained than the upstream area, as confirmed by the presence of a large island and a secondary channel on the right side. During severe floods, therefore, the main channel can migrate forming new deposition bars. On the other hand, the dynamics of Fontaniva are related to: i) greater availability of eroded sediment coming from the upper sub-reaches; ii) more balanced erosion-deposition pattern (Moretto et al., 2012a,b, 2013b); iii) increase in the average elevation of the active channel in the last 30 years; iv) presence of extended and stable vegetation in the floodplain area which is increasingly affected by flood events; v) reduction of local slope; vi) presence of infrastructures (2 bridges). The reduction of slope, together with the vertical aggradation of the active channel over the last 30 years (Moretto et al., 2012a,b, 2013b), determine a greater lateral mobility due to flood events, especially on the banks with dense and stable riparian vegetation (Fig. 1).

The morphological changes that occurred in the Brenta River as a consequence of the flood events in 2010 (RI of about 8 and 10 years) are of interest to evaluate the fluvial hydro-morphological quality, because they highlight the processes that are taking place, and provide insights for their future evolution as required by the EU Water Framework Directive. Nevertheless, the implementation of evolutionary models and the estimation of sediment transport require a better assessment of the quantity of incoming and outbound sediment in the study reach and a detailed analysis of the transport rate in relation to the event magnitude. Several studies tried to apply the morphological approach for estimating sediment budget starting from transversal sections (i.e. Bertoldi et al., 2010; Lane, 1998; Surian and Cisotto, 2007), even if a much more accurate spatial definition can be obtained from remote sensing data (i.e. Hicks, 2012; Hicks et al., 2006; Milan and Heritage, 2012; Rennie, 2012). The traditional methodologies of terrain change detection (e.g. with dGPS cross-sections) provide higher local precision, but the determination of volume changes at reach scale may be improved with the assessment of DEMs differences (Lane et al., 2003). The implementation of LiDAR data and colour bathymetry with the proposed methodology allowed us to obtain a terrain digital model with sufficient accuracy to derive patterns of sediment transfer, in particular within the water channels. The information obtained from such analyses should be integrated with direct field measurements.

6. Final remarks

The proposed methodology allows the production of high-resolution DTMs of wet areas with an associated uncertainty that has proved to be comparable to the LiDAR data up to 1–1.20 m of water depth. The bathymetric model calibration requires only a dGPS survey in the wet areas taken during aerial image acquisition. Statistical analyses have demonstrated that all three colour bands (R, G, B) significantly correlate with water depth with a good performance of the empirical models. In addition, the presence of an interaction between the colour bands cannot be neglected. This study supports the evidence that, in a complex gravel-bed river with different water depths and different colours on channel bottom, the tested physical models have a lower degree of significance in respect to the empirical models. Different errors were identified on raw HDTM: light reflections, water turbulences, strong colour variations at the bottom, periphyton, shadows, suspended load, exposed sediment and submerged vegetation.

Error sources were mostly intercepted through two proposed filters which consider curvature assessment and implausible upper and lower limits in the bathymetric raster. As a consequence, a preliminary analysis seems to be needed to assess in advance both the percentage of wet surface and the range of depths in the river reach to be surveyed in order to reduce the number of calibration points for each water depth class, thus allowing a fairly acceptable error for the major part of the wet areas.

The validation of the Hybrid Digital Terrain Models (HDTM) resulted satisfactory for distributed evaluations of morphological variations. The bathymetric method proved to be fundamental to obtain realistic evaluations when aiming at quantifying erosion–deposition patterns, applying numerical models to simulated floods or developing sediment budgets.

The flood events of November–December 2010 (RI = 8 and 10 years) have caused significant geomorphic changes in all three sub-reaches. The different behaviour among the sub-reaches seems to be attributable to their diverse morphological characteristics and the availability of sediment from upstream. A predominance of erosion processes, with a consequent negative balance between deposition and erosion at sub-reach level decreasing when going from the upper reach ($-104{,}082\ m^3$) to the lower one ($-45{,}232\ m^3$), was found. Riffle–pool dynamics seem influenced by the nature of lateral constriction (natural banks vs. embankments and bridges). After a severe flood event, pools seem be located mainly near compact banks with embankments and/or vegetated bars. On the other hand, riffles seem to be located mainly where no significant constrictions were present on either side of the wet areas.

The results of this study can be a valuable support to generate precise elevation models also for wet areas, useful for evaluating erosion–deposition patterns, improving sediment budget calculations and the implementation of 2D and 3D numerical hydrodynamic models.

Notation

dGPS	Differential Global Positioning System
DEM	Digital Elevation Model
DPH	Channel Depth [*m*]
DTM	Digital Terrain Model
HDTM	Hybrid Digital Terrain Model
LiDAR	Light Detection And Ranging
RDPH	Raw channel depth model (raster and/or points)
RGB	Red Green Blue
RI	Recurrence Interval [*years*]
Zdry	Z coordinate of dry area [*m.a.s.l.*]
Zwet	Z coordinate of wet area [*m.a.s.l.*]
Zw	Z coordinate of water level [*m.a.s.l.*]

Acknowledgements

This research was funded by the CARIPARO Research Project "Linking geomorphological processes and vegetation dynamics in gravel-bed rivers"; the University of Padua Strategic Research Project PRST08001, "GEORISKS, Geological, morphological and hydrological processes: monitoring, modelling and impact in North-Eastern Italy", Research Unit STPD08RWBY-004; the Italian National Research Project PRIN20104ALME4-ITSedErosion: "National network for monitoring, modelling and sustainable management of erosion processes in agricultural land and hilly-mountainous area"; and the EU SedAlp Project: "Sediment management in Alpine basins: Integrating sediment continuum, risk mitigation and hydropower", 83-4-3-AT, within the framework of the European Territorial Cooperation Programme Alpine Space 2007–2013. All colleagues and students who helped in the field are sincerely thanked. Thanks to mother tongue Ms Alison Garside for the efficient English correction of the final English version and for the final paper check.

References

Ashmore, P.E., Church, M.J., 1998. Sediment transport and river morphology: a paradigm for study. In: Kingleman, P.C., Bechta, R.L., Komar, P.D., Bradley, J.B. (Eds.), Gravel Bed

Rivers in the Environment. Highland Ranch, CO, Water Resources Publications, pp. 115–148.
Bathurst, J.C., Crosta, G.B., Garcìa Ruiz, J.M., Guzzetti, F., Lenzi, M.A., Aragues, S., 2003. Debris fall assessment in mountain catchments for local End-users. International Conference on Debris Flow Hazards Mitigation: Mechanics, Prediction and Assessment, Proceedings 2, pp. 1073–1083.
Bertoldi, W., Gurnell, A., Surian, N., Tockner, K., Zanoni, L., Ziliani, L., Zolezzi, G., 2009. Understanding reference processes: linkages between river flows, sediment dynamics and vegetated landforms along the Tagliamento River, Italy. River Res. Appl. 25, 501–516.
Bertoldi, W., Zanoni, L., Tubino, M., 2010. Assessment of morphological changes induced by flow and flood pulses in a gravel bed braided river: the Tagliamento River (Italy). Geomorphology 114, 348–360.
Brasington, J., Rumsby, B.T., McVey, R.A., 2000. Monitoring and modelling morphological change in a braided gravel-bed river using high resolution GPS-based survey. Earth Surf. Process. Landf. 25 (9), 973–990.
Brasington, J., Langham, J., Rumsby, B., 2003. Methodological sensitivity of morphometric estimates of coarse fluvial sediment transport. Geomorphology 53 (3), 299–316.
Brasington, J., Vericat, D., Rychkov, I., 2012. Modeling river bed morphology, roughness, and surface sedimentology using high resolution terrestrial laser scanning. Water Resour. Res. 48 (11). http://dx.doi.org/10.1029/2012WR012223.
Buffington, J.M., 2012. Change in channel morphology over human time scales. In: Church, M., Biron, P.M., Roy, A.G. (Eds.), Gravel-bed Rivers: Processes, Tool, Environments. Wiley-Blackwell, pp. 435–463.
Burnham, K.P., Anderson, D.R., 2002. 2nd ed. Model Selection and Multimodel Inference: A Practical Information-Theoretic Approach, 16. Springer, p. 488.
Carbonneau, P.E., Lane, S.N., Bergeron, N.E., 2006. Feature based image processing methods applied to bathymetric measurements from airborne remote sensing in fluvial environments. Earth Surf. Process. Landf. 31, 1413–1423. http://dx.doi.org/10.1002/esp.1341.
Cavalli, M., Tarolli, P., 2011. Application of LiDAR technology for rivers analysis. Ital. J. Eng. Geol. Environ. 11, 33–44.
Charlton, M.E., Large, A.R., Fuller, I.C., 2003. Application of airborne LiDAR in river environments: the River Coquet, Northumberland, UK. Earth Surf. Process. Landf. 28 (3), 299–306.
Comiti, F., 2011. How natural are Alpine mountain rivers? Evidence from the Italian Alps. Earth Surf. Process. Landf. 37, 693–707. http://dx.doi.org/10.1002/esp.2267.
Comiti, F., Da Canal, M., Surian, N., Mao, L., Picco, L., Lenzi, M.A., 2011. Channel adjustments and vegetation cover dynamics in a large gravel bed river over the last 200 years. Geomorphology 125, 147–159.
Conesa-Garcìa, C., Lenzi, M.A., 2013. Check Dams, Morphological Adjustments and Erosion Control in Torrential Streams. Nova Science Publishers, Inc., New York 978-1-60876-146-3, pp. 1–339.
Delai, F., Moretto, J., Picco, L., Rigon, E., Ravazzolo, D., Lenzi, M.A., 2014. Analysis of morphological processes in a disturbed gravel-bed river (Piave River): integration of LiDAR data and colour bathymetry. J. Civil Eng. Archit. 8 (5), 639–648 (ISSN 1934-7359).
Dierssen, H.M., Zimmerman, R.C., Leathers, R.A., Downes, T.V., Davis, C.O., 2003. Ocean color remote sensing of seagrass and bathymetry in the Bahamas Banks by high-resolution airborne imagery. Limnol. Oceanogr. 48 (1, part 2), 444–455.
Dixon, L.F.J., Barker, R., Bray, M., Farres, P., Hooke, J., Inkpen, R., Merel, A., Payne, D., Shelford, A., 1998. Analytical photogrammetry for geomorphological research. In: Lane, S.N., Richards, K.S., Chandler, J.H. (Eds.), Landform Monitoring, Modelling and Analysis. John Wiley & Sons, Chichester, pp. 63–94 (Chapter 4).
Fewtrell, T.J., Duncan, A., Sampson, C.C., Neal, J.C., Bates, P.D., 2011. Benchmarking urban flood models of varying complexity and scale using high resolution terrestrial LiDAR data. Phys. Chem. Earth A/B/C 36 (7), 281–291.
Fryer, J.G., 1983. A simple system for photogrammetric mapping in shallow-water. Photogramm. Rec. 11, 203–208.
Heritage, G.L., Fuller, I.C., Charlton, M.E., Brewer, P.A., Passmore, D.P., 1998. CDW photogrammetry of low relief fluvial features: accuracy and implications for reach-scale sediment budgeting. Earth Surf. Process. Landf. 23, 1219–1233.
Hicks, D.M., 2012. Remotely sensed topographic change in gravel riverbeds with flowing channels. In: Church, M., Biron, P.M., Roy, A.G. (Eds.), Gravel-bed Rivers: Processes, Tool, Environments. Wiley-Blackwell, pp. 303–314.
Hicks, D.M., Duncan, M.J., Walsh, J.M., Westaway, R.M., Lane, S.N., 2002. New views of the morphodynamics of large braided rivers from high-resolution topographic surveys and time-lapse video. IAHS Publ. 276, 373–380.
Hicks, D.M., Shankar, U., Duncan, M.J., Rebuffe, M., Abele, J., 2006. Use of remote sensing technologies to assess impacts of hydro-operations on a large, braided, gravel-bed river: Waitaki River, New Zealand. In: Sambrook Smith, G.H., Best, J.L., Bristow, C.S., Petts, G.E. (Eds.), Braided Rivers, Processes, Deposits, Ecology and Management. International Association of Sedimentologists, Special Publication, 36. Blackwell, Oxford, pp. 311–326.
Hilldale, R.C., Raff, D., 2008. Assessing the ability of airborne LiDAR to map river bathymetry. Earth Surf. Process. Landf. 33, 773–783.
Kaless, G., Mao, L., Lenzi, M.A., 2011. Regime theories in gravel bed rivers; preliminary comparison between disturbed rivers due to antrophic activities (Northeastern Italy) and natural rivers (Patagonia, Argentina). Proceedings of the Intermediate Congress of the Italian Association of Agricultural Engineering; Belgirate, Italy; September 22–24, 2011, p. 8.
Kaless, G., Mao, L., Lenzi, M.A., 2014. Regime theories in gravel bed rivers: models, controlling variables, and applications in disturbed Italian rivers. Hydrol. Process. 28, 2348–2360. http://dx.doi.org/10.1002/hyp.9775.
Kinzel, P.J., Wright, C.W., Nelson, J.M., Burman, A.R., 2007. Evaluation of an experimental LiDAR for surveying a shallow, braided, sand-bedded river. J. Hydraul. Eng. 133, 838–842.
Kinzel, P.J., Legleiter, C.J., Nelson, J.M., 2013. Mapping River Bathymetry With a Small Footprint Green LiDAR: applications and Challenges. J. Am. Water Resour. Assoc. 49, 183–204. http://dx.doi.org/10.1111/jawr.12008.
Lane, S.N., 1998. The use of digital terrain modelling in the understanding of dynamic river channel systems. In: Lane, S.N., Richards, K., Chandler, J. (Eds.), Landform Monitoring, Modelling and Analysis. Wiley, Chichester, pp. 311–342.
Lane, S.N., Richards, K.S., Chandler, J.H., 1994. Developments in monitoring and terrain modelling of small-scale riverbed topography. Earth Surf. Process. Landf. 19, 349–368.
Lane, S.N., Westaway, R.M., Hicks, D.M., 2003. Estimation of erosion and deposition volumes in a large, gravel-bed, braided river using synoptic remote sensing. Earth Surf. Process. Landf. 28 (3), 249–271. http://dx.doi.org/10.1002/esp.483.
Lane, S.N., Tayefi, V., Reid, S.C., Yu, D., Hardy, R.J., 2007. Interactions between sediment delivery, channel change, climate change and flood risk in a temperate upland environment. Earth Surf. Process. Landf. 32, 429–446.
Lane, S.N., Widdison, P.E., Thomas, R.E., Ashworth, P.J., Best, J.L., Lunt, I.A., Sambrook Smith, G.H., Simpson, C.J., 2010. Quantification of braided river channel change using archival digital image analysis. Earth Surf. Process. Landf. 35, 971–985. http://dx.doi.org/10.1002/esp.2015.
Legleiter, C.J., 2011. Remote measurement of river morphology via fusion of LiDAR topography and spectrally based bathymetry. Earth Surf. Process. Landf. 37, 499–518.
Legleiter, C.J., 2013. Mapping river depth from publicly available aerial images. River Res. Appl. 29, 760–780. http://dx.doi.org/10.1002/rra.2560.
Legleiter, C.J., Roberts, D.A., 2009. A forward image model for passive optical remote sensing of river bathymetry. Remote Sens. Environ. 113, 1025–1045.
Legleiter, C.J., Roberts, D.A., Marcus, W.A., Fonstad, M.A., 2004. Passive optical remote sensing of river channel morphology and in-stream habitat: physical basis and feasibility. Remote Sens. Environ. 93, 493–510.
Legleiter, C.J., Roberts, D.A., Lawrence, R.L., 2009. Spectrally based remote sensing of river bathymetry. Earth Surf. Process. Landf. 34, 1039–1059.
Legleiter, C.J., Kinzel, P.J., Overstreet, B.T., 2011. Evaluating the potential for remote bathymetric mapping of a turbid, sand-bed river: 1. Field spectroscopy and radiative transfer modeling. Water Resour. Res. 4, W09531.
Lenzi, M.A., 2006. Research developments in debris flow monitoring, modeling and hazard assessment in Italian mountain catchments. WIT Trans. Ecol. Environ. 90, 135–145.
Lenzi, M.A., D'Agostino, V., Gregoretti, C., Sonda, D., 2003. A simplified numerical model for debris-flow hazard assessment: DEFLIMO. International Conference on Debris Flow Hazards Mitigation: Mechanics, Prediction and Assessment, Proceedings 1, pp. 611–622.
Lenzi, M.A., Mao, L., Comiti, F., Rigon, E., Picco, L., Vitti, P., Moretto, J., Sigolo, C., 2010. Scientific contribution by the Research Unit Land and Agro-forest Department, to the research activities carried out in the framework of the CARIPARO Project "Linking geomorphological processes and vegetation dynamics in gravel-bed rivers", from September 2009 to October 2010. Research and Technical Report. Department of Land and Agro-forest Environment, University of Padova, Padova, Italy, p. 102.
Macklin, M.G., Rumsby, B.T., 2007. Changing climate and extreme floods in the British uplands. Trans. Inst. Br. Geogr. 32, 168–186. http://dx.doi.org/10.1111/j.1475-5661.2007.00248.x.
Mao, L., Lenzi, M.A., 2007. Sediment mobility and bedload transport conditions in an alpine stream. Hydrol. Process. 21 (14), 1882–1891.
Mao, L., Cavalli, M., Comiti, F., Marchi, L., Lenzi, M.A., Arattano, M., 2009. Sediment transfer processes in two Alpine catchments of contrasting morphology settings. J. Hydrol. 364, 88–98.
Marcus, W.A., 2012. Remote sensing of the hydraulic environments in gravel-bed rivers. In: Church, M., Biron, P.M., Roy, A.G. (Eds.), Gravel-bed Rivers: Processes, Tool, Environments. Wiley-Blackwell, pp. 261–285.
Marcus, W.A., Fonstad, M.A., 2008. Optical remote mapping of rivers at sub-meter resolutions and watershed extents. Earth Surf. Process. Landf. 33, 4–24.
Marcus, W.A., Legleiter, C.J., Aspinall, R.J., Boardman, J.W., Crabtree, R.L., 2003. High spatial resolution hyperspectral mapping of in-stream habitats, depths, and woody debris in mountain streams. Geomorphology 55, 363–380.
McKean, J.A., Nagel, D., Tonina, D., Bailey, P., Wright, C.W., Bohn, C., Nayegandhi, A., 2009. Remote sensing of channels and riparian zones with a narrow-beam aquatic-terrestrial LIDAR. Remote Sens. 1 (4), 1065–1096.
Milan, D.J., Heritage, G.L., 2012. LiDAR and ADCP use in gravel-bed rivers: advances since GBR6. In: Church, M., Biron, P.M., Roy, A.G. (Eds.), Gravel-bed Rivers: Processes, Tool, Environments. Wiley-Blackwell, pp. 286–302.
Milan, D.J., Heritage, G.L., Hetherington, D., 2007. Application of a 3D laser scanner in the assessment of erosion and deposition volumes and channel change in a proglacial river. Earth Surf. Process. Landf. 32, 1657–1674.
Milan, D.J., Heritage, G.L., Large, A.R.G., Fuller, I.C., 2011. Filtering spatial error from DEMs: implications for morphological change estimation. Geomorphology 125, 160–171.
Moore, I.D., Grayson, R.B., Landson, A.R., 1991. Digital terrain modelling: a review of hydrological, geomorphological, and biological applications. Hydrol. Process. 5, 3–30.
Moretto, J., Rigon, E., Mao, L., Picco, L., Delai, F., Lenzi, M.A., 2012a. Medium-and short-term channel and island evolution in a disturbed gravel bed river (Brenta River, Italy). J. Agric. Eng. 43 (4), 176–188. http://dx.doi.org/10.4081/jae.2012.e27.
Moretto, J., Rigon, E., Mao, L., Picco, L., Delai, F., Lenzi, M.A., 2012b. Assessing short term erosion-deposition processes of the Brenta River using LiDAR survey. WIT Trans. Eng. Sci. 73, 149–160. http://dx.doi.org/10.2495/DEB120131.
Moretto, J., Delai, F., Picco, L., Lenzi, M.A., 2013a. Integration of colour bathymetry, LiDAR and dGPS surveys for assessing fluvial changes after flood events in the Tagliamento River (Italy). Agric. Sci. 4 (8A), 21–29. http://dx.doi.org/10.4236/as.2013.48A004.

Moretto, J., Rigon, E., Mao, L., Picco, L., Delai, F., Lenzi, M.A., 2013b. Channel adjustment and island dynamics in the Brenta River (Italy) over the last 30 years. River Res. Appl. http://dx.doi.org/10.1002/rra.2676.

Muste, M., Kim, D., Merwade, V., 2012. Modern digital instruments and techniques for hydrodynamic and morphologic characterization of river channels. In: Church, M., Biron, P.M., Roy, A.G. (Eds.), Gravel-bed Rivers: Processes, Tool, Environments. Wiley-Blackwell, pp. 315–341.

Panissod, F., Bailly, J.S., Durrieu, S., Jacome, A., Mathys, N., Cavalli, M., Puech, C., 2009. Qualifiction de modeles numeriques de terrain Lidar pour l'etude de l'erosion: Application aux badlands de draix. Rev. Fr. Photogramm. Teledetection 192, 50–57.

Picco, L., Mao, L., Rigon, E., Moretto, J., Ravazzolo, D., Delai, F., Lenzi, M.A., 2012a. Medium term fluvial island evolution in relation with floods events in the Piave River. WIT Trans. Eng. Sci. vol. 73, 161–172. http://dx.doi.org/10.2495/DEB120141 (ISSN 1743–3522).

Picco, L., Mao, L., Rigon, E., Moretto, J., Ravazzolo, D., Delai, F., Lenzi, M.A., 2012b. Riparian forest structure, vegetation cover and flood events in the Piave River. WIT Trans. Eng. Sci. 73, 137–147. http://dx.doi.org/10.2495/DEB120121 (ISSN 1743–3522).

Picco, L., Mao, L., Cavalli, M., Buzzi, R., Rainato, R., Lenzi, M.A., 2013. Evaluating short-term morphological changes in a gravel-bed braided river using Terrestrial Laser Scanner. Geomorphology 201, 323–334. http://dx.doi.org/10.1016/j.geomorph.2013.07.007.

Picco, L., Mao, L., Rainato, R., Lenzi, M.A., 2014. Medium-term fluvial island evolution in a disturbed gravel-bed river (Piave River, Northeastern Italian Alps). Geogr. Ann. Ser. A Phys. Geogr. 96, 83–97. http://dx.doi.org/10.1111/geoa.12034.

Rennie, C.D., 2012. Mapping water and sediment flux distributions in gravel-bed rivers using ADCPs. In: Church, M., Biron, P.M., Roy, A.G. (Eds.), Gravel-bed Rivers: Processes, Tool, Environments. Wiley-Blackwell, pp. 342–350.

Rigon, E., Comiti, F., Mao, L., Lenzi, M.A., 2008. Relationships among basin area, sediment transport mechanisms and wood storage in mountain basins of the Dolomites (Italian Alps). WIT Trans. Eng. Sci. 60, 163–172.

Rigon, E., Comiti, F., Lenzi, M.A., 2012. Large wood storage in streams of the Eastern Italian Alps and the relevance of hillslope process. Water Resour. Res. 48, W01518. http://dx.doi.org/10.1025/2010 WR009854.

Rinner, K., 1969. Problems of two medium photogrammetry. Photogramm. Eng. 35, 275.

Rumsby, B.T., Macklin, M.G., 1994. Channel and floodplain response to recent abrupt climate change: the Tyne basin, Northern England. Earth Surf. Process. Landf. 19 (6), 499–515.

Rumsby, B.T., Brasington, J., Langham, J.A., McLelland, S.J., Middleton, R., Rollingson, G., 2008. Monitoring and modelling particle and reach-scale morphological change in gravel-bed rivers: applications and challenges. Geomorphology 93 (1), 40–54.

Sampson, C.C., Fewtrell, T.J., Duncan, A., Shaad, K., Horritt, M.S., Bates, P.D., 2012. Use of terrestrial laser scanning data to drive decimetric resolution urban inundation models. Adv. Water Resour. 41, 1–17.

Smith, M.W., Vericat, D., 2013. Evaluating shallow-water bathymetry from through-water terrestrial laser scanning under a range of hydraulic and physical water quality conditions. River Res. Appl. http://dx.doi.org/10.1002/rra.2687 (published online 10 July 2013).

Smith, M., Vericat, D., Gibbins, C., 2012. Through water terrestrial laser scanning of gravel beds at the patch scale. Earth Surf. Process. Landf. 37 (4), 411–421.

Stover, S.C., Montgomery, D.R., 2001. Channel change and flooding, Skokomish River, Washington. J. Hydrol. 243, 272–286.

Surian, N., Cisotto, A., 2007. Channel adjustments, bedload transport and sediment sources in a gravel-bed river, Brenta river, Italy. Earth Surf. Process. Landf. 32, 1641–1656.

Surian, N., Ziliani, L., Comiti, F., Lenzi, M.A., Mao, L., 2009. Channel adjustments and alteration of sediment fluxes in gravel-bed rivers of north-eastern Italy: potentials and limitations for channel recovery. River Res. Appl. 25, 551–567.

Taylor, J., 1997. An Introduction to Error Analysis: The Study of Uncertainties in Physical Measurements, 2nd ed. University Science Books, Sausalito, CA.

Wheaton, J.M., Brasington, J., Darby, S.E., Sear, D.A., 2010. Accounting for uncertainty in DEMs from repeat topographic surveys: improved sediment budgets. Earth Surf. Process. Landf. 35, 136–156.

Wheaton, J.M., Brasington, J., Darby, S.E., Kasprak, A., Sear, D., Vericat, D., 2013. Morphodynamic signatures of braiding mechanisms as expressed through change in sediment storage in a gravel-bed river. J. Geophys. Res. Earth Surf. 118 (2), 759–779.

Williams, R.D., Brasington, J., Vericat, D., Hicks, D.M., Labrosse, F., Neal, M., 2011. Monitoring braided river change using terrestrial laser scanning and optical bathymetric mapping. In: Smith, M., Paron, P., Griffiths, J. (Eds.), Geomorphological Mapping. Elsevier, Oxford, pp. 507–531.

Williams, R.D., Brasington, J., Hicks, M., Measures, R., Rennie, C.D., Vericat, D., 2013. Hydraulic validation of two-dimensional simulations of braided river flow with spatially continuous aDcp data. Water Resour. Res. 49 (9), 5183–5205.

Williams, R.D., Brasington, J., Vericat, D., Hicks, D.M., 2014. Hyperscale terrain modelling of braided rivers: fusing mobile terrestrial laser scanning and optical bathymetric mapping. Earth Surf. Process. Landf. 39 (2), 167–183.

Winterbottom, S.J., Gilvear, D.J., 1997. Quantification of channel bed morphology in gravel-bed rivers using airborne multispectral imagery and aerial photography. Regul. Rivers Res. Manag. 13, 489–499.